Results

Immunohistochemistry of DMP1 in rat bone

To characterize the polyclonal antibodies against the rat DMP1-1, DMP1-2, DMP1-3, and DMP1-4 peptides, we performed immunohistochemistry on rat bones using these antibodies. Analyses using anti-DMP1-1 or -DMP1-2 antibodies revealed immunoreactivity in the osteocytes and their surrounding bone matrix (Figs. 2a, b). By contrast, analyses using anti-DMP1-3 or -DMP1-4 antibodies revealed immunoreactivity in the pericanalicular matrix rather than in osteocytes (Figs. 2c, d). All these antibodies revealed no immunoreactivity in osteoblasts (Figs. 2a–d). These patterns of immunoreactivity in osteocytes and osteocyte-related matrix were consistent with the previously reported osteocytic expression of DMP1. From these observations, we concluded that the polyclonal antibodies correctly recognize local DMP1 in the bone.

Identification of circulating DMP1 in blood

To confirm the presence of DMP1 in circulating blood, we extracted immunoreactive products from rat plasma by affinity chromatography using antibodies against DMP1-1 or DMP1-3, and analyzed these products by LC-MS/MS. The LC-MS spectra of the immunoreactive products affinity-extracted with the polyclonal antibody against DMP1-1 (which recognizes for NH_2-terminal fragments of DMP1) revealed the YQNTESESSEER, SEESKGDHEPTSTQDSDDSQDVEFSSR, and SKEESNSTGSTSSSEEDNHPK peptides of rat DMP1 (Fig. 1). Likewise, the LC-MS spectra of the immunoreactive products affinity-extracted with the polyclonal antibody against DMP1-3 (which recognizes COOH-terminal fragments of DMP1) revealed the same three peptides. These findings confirmed that DMP1 was present in circulating blood, and that these antibodies could detect the circulating DMP1.

Development and characteristics of rat DMP1 immunoassay

Previous studies demonstrated that cleavages at four sites within DMP1 produce NH_2- and COOH-terminal fragments, with only a small amount of DMP1 remaining uncleaved [4,5]. In fact, ELISA using pairs of antibodies that recognized uncleaved DMP1 did not have sufficient sensitivity to detect circulating DMP1 (data not shown). We selected pairs of antibodies that recognized either the NH_2- or COOH-terminal fragments. In sandwich ELISA 1–2, polyclonal antibodies against the DMP1-1 and DMP1-2 peptides of the NH_2-terminal fragment were used, with anti-DMP1-1 as the capture antibody and HRP-conjugated anti-DMP1-2 as the detection antibody (Fig. 1). In sandwich ELISA 4–3, polyclonal antibodies against the DMP1-3 and DMP1-4 peptides of the COOH-terminal fragment were used, with anti-DMP1-4 as the capture antibody and HRP-conjugated anti-DMP1-3 as the detection antibody (Fig. 1). Dilutions of recombinant rat DMP1 were used for the standard curve.

The sensitivity of the assay was calculated to be 4.04 pg/mL for ELISA 1–2 and 2.51 pg/mL for ELISA 4–3 using NCCLS methods. The precision was determined using three spiked QC samples (high, middle, and low). Intra-assay variations ($n = 24$) were less than 5.7% for ELISA 1–2 (Table 1) and less than 8.6% for ELISA 4–3 (Table 2), and inter-assay variations ($n = 6$) were less than 6.3% for ELISA 1–2 (Table 1) and less than 8.2% for ELISA 4–3 (Table 2). Blood samples, collected either as EDTA plasma or serum, exhibited no appreciable differences in the detectable concentration of immunoreactive DMP1 (data not shown). Dilution

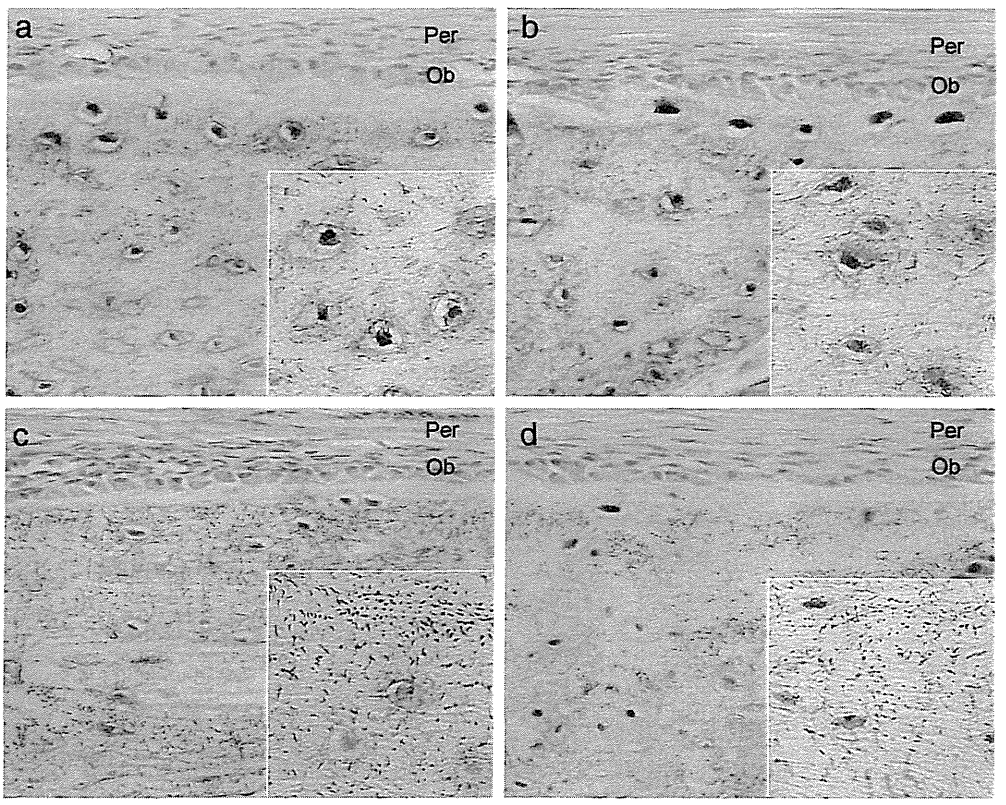

Fig. 2. Immunohistochemistry of local DMP1 in rat bone. (a) Immunostaining with antibody against DMP1-1 was seen in osteocytes and their surrounding bone matrix. (b) Immunostaining with antibody against DMP1-2 was seen in osteocytes and their surrounding bone matrix. (c) Immunostaining with antibody against DMP1-3 was seen in pericanalicular matrix rather than in osteocytes. (d) Immunostaining with antibody against DMP1-4 was seen in pericanalicular matrix rather than in osteocytes. (a)–(d) Immunostaining with antibodies against DMP1-1, 2, 3, 4 was not seen in osteoblasts. Insets in (a)–(d) show a higher magnification of osteocytes. Ob; osteoblast, Per; periosteum. Counterstaining was performed with hematoxylin. Original magnification, ×400. (Inset) Original magnification, ×700.

Table 1
Intra- and interassay precision of three control rat plasma samples in DMP1 ELISA 1-2.

	Intraassay variation (n = 24)		Interassay variation (n = 6)	
	Mean ± SD		Mean ± SD	
Sample	(pg/mL)	CV (%)	(pg/mL)	CV (%)
Low control	81.5 ± 3.74	4.6	83.8 ± 5.31	6.3
Medium control	306.5 ± 13.64	4.5	307.0 ± 13.29	4.3
High control	1049.1 ± 59.39	5.7	1081.3 ± 36.36	3.4

n: number of determinations
SD: standard deviation
CV: coefficient of variation

Table 2
Intra- and interassay precision of three control rat plasma samples in DMP1 ELISA 4-3.

	Intraassay variation (n = 24)		Interassay variation (n = 6)	
	Mean ± SD		Mean ± SD	
Sample	(pg/mL)	CV (%)	(pg/mL)	CV (%)
Low control	90.1 ± 7.78	8.6	87.0 ± 7.13	8.2
Medium control	306.0 ± 18.75	6.1	318.6 ± 23.57	7.4
High control	1045.7 ± 68.87	6.6	1121.5 ± 50.90	4.5

n: number of determinations
SD: standard deviation
CV: coefficient of variation

linearity was determined from three plasma samples (from 12, 18, and 96-week-old rats) in triplicate after serial dilution (ranging from 1:16 to 1:1024) with assay buffer; graphs of these were approximately parallel to the standard curve (Fig. 3). Plasma samples from three normal rats were incubated at 4 °C for 24 h or 37 °C for 1 h, and the DMP1 levels in these plasma samples were compared with those of the same plasma samples stored at −80 °C. In ELISA 1-2, the DMP1 concentration in plasma of 12-week-old rats incubated at 4 °C and 37 °C was 97.7 ± 20.9% (mean ± SD) and 99.0 ± 21.5% (mean ± SD) of the concentration in control plasma stored at −80 °C. In ELISA 4-3, the DMP1 concentration in plasma of 12-week-old rats incubated at 4 °C and 37 °C was 94.5 ± 21.3% (mean ± SD) and 91.3 ± 18.5% (mean ± SD) of the concentration in control plasma stored at −80 °C.

Studies in which recombinant rat DMP1 was added to 40- or 80-fold diluted rat EDTA plasma, yielded recoveries of 90.5–92.2% in ELISA 1-2 (Table 3) and 96.2–97.1% in ELISA 4-3 (Table 4). Studies in which recombinant rat DMP1 was added to 40- or 80-fold diluted rat serum, yielded recoveries of 90.7–95.2% in ELISA 1-2 (Table 3) and of 97.1–97.6% in ELISA 4-3 (Table 4).

Table 3
Recovery of rat DMP1 in ELISA 1-2.

Sample no.	Theoretical value (pg/mL)	Measured value (pg/mL)	Recovery (%)
Rat EDTA plasma			
Sample 1	537.7	486.8	90.5
Sample 2	459.6	423.7	92.2
Sample 3	420.5	386.0	91.8
Rat serum			
Sample 4	959.3	889.3	92.7
Sample 5	881.2	838.8	95.2
Sample 6	842.1	763.5	90.7

Table 4
Recovery of rat DMP1 in ELISA 4-3.

Sample no.	Theoretical value (pg/mL)	Measured value (pg/mL)	Recovery (%)
Rat EDTA plasma			
Sample 1	1342.8	1303.4	97.1
Sample 2	1264.7	1217.1	96.2
Sample 3	1225.7	1182.5	96.5
Rat serum			
Sample 4	2179.6	2126.4	97.6
Sample 5	2101.5	2041.7	97.2
Sample 6	2062.4	2002.2	97.1

Age-associated decrease of circulating DMP1 levels in male rats

We determined reference levels for circulating DMP1 in normal male rats of various ages (2–96 weeks). Both ELISA 1-2 and ELISA 4-3 showed that circulating DMP1 concentrations significanlly decrease with age (Fig. 4). During rapid skeletal growth (2–12 weeks), mean DMP1 values measured by ELISA 4-3 were over three times higher than those measured by ELISA 1-2. However, mean DMP1 values in old animals (72 and 96 weeks) were almost the same when measured by either ELISA.

Correlations between levels of DMP1 and other biochemical markers

We also measured the levels of the other biochemical markers of bone metabolism in normal male rats of various ages (2–96 weeks) (Fig. 5) and assessed the correlations between the levels of DMP1 and these other markers. Both osteocalcin and Dkk-1 levels tended to decrease with age. Both Trap5b and SOST levels were increased at 8 weeks and decreased after 12 weeks. Among all bone markers,

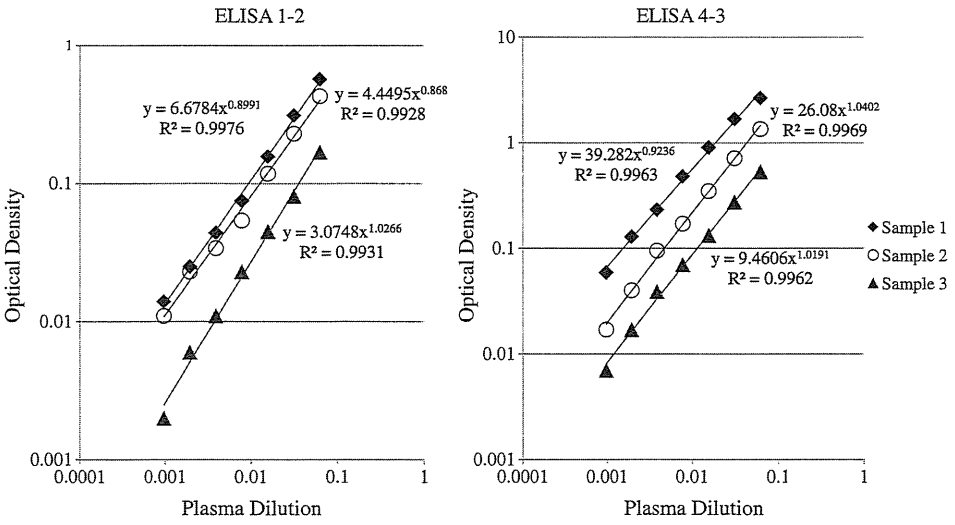

Fig. 3. Linearity of dilution studied in rat DMP1 ELISA assays. Each data point of ELISA 1-2 (left) or ELISA 4-3 (right) represents the mean of three separate measurements. Linear regression equations, together with the squares of the correlation coefficients (R^2), are shown.

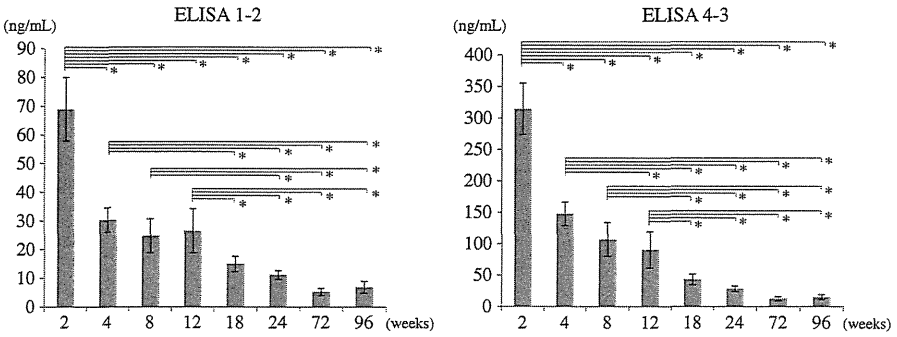

Fig. 4. DMP1 concentrations in plasma from male rats of various ages. Circulating DMP1 concentrations were evaluated in 2- (n = 5), 4- (n = 5), 8- (n = 6), 12- (n = 6), 18- (n = 6), 24- (n = 5), 72- (n = 5), and 96- (n = 5) week-old male Wistar rats by DMP1 ELISA 1–2 (left) and ELISA 4–3 (right). Values are expressed as means ± SD of DMP1 concentrations at each age. All comparisons between results from different age groups are shown, with $p < 0.05$ indicating a significant difference (*).

DMP1 levels measured by ELISA 1–2 had the highest positive correlation with DMP1 levels measured by ELISA 4–3 (Table 5). Among the other biochemical markers, DMP1 levels measured by both ELISAs 1–2 and 4–3 had the highest positive correlation with levels of Dkk-1, and the second highest positive correlation with the levels of osteocalcin; DMP1 levels were less highly correlated with the levels of Trap5b and SOST (Table 5).

Discussion

DMP1 is a noncollagenous bone matrix proteins produced by osteocytes [1]. Due to its highly acidic nature, DMP1 can bind to calcium, thereby regulating matrix mineralization [3]. Observations made in DMP1-null mice and humans with DMP1 mutations associated with autosomal-recessive hypophosphatemic rickets (ARHR) have shown that impairment of DMP1 results in elevated serum FGF23, which regulates phosphate homeostasis, and in pathological changes of bone mineralization [6,7]. However, the biological function of DMP1 is not yet fully understood. Considering that DMP1 is predominantly produced in osteocytes, whereas other bone matrix proteins such as osteocalcin, osteopontin, and bone sialoprotein are produced in osteoblasts [1,15–17], DMP1 in circulating blood is a candidate marker for osteocyte activity. To investigate the biological significance of DMP1, we developed new sandwich ELISAs for measuring rat DMP1 and used these assays to monitor age-related changes in circulating DMP1 levels. In addition, we analyzed the correlations between levels of DMP1 and other biochemical markers of bone metabolism.

We developed sandwich ELISAs for rat DMP1 using two pairs of polyclonal antibodies with high affinity to rat DMP1. These polyclonal antibodies were characterized by immunohistochemical and LC-MS/MS studies. In immunohistochemical analyses of rat bone using these antibodies, we observed immunoreactivity in osteocytes and pericanalicular matrix, as previously reported. LC-MS/MS analyses of rat plasma-derived immunoreactive products affinity-extracted with our polyclonal antibodies revealed the presence of DMP1 in circulating blood. It is generally accepted that a small fraction of bone matrix protein, such as osteocalcin, is released from the bone into the circulation, where it can be detected by immunoassay [8]. Similarly, a small fraction

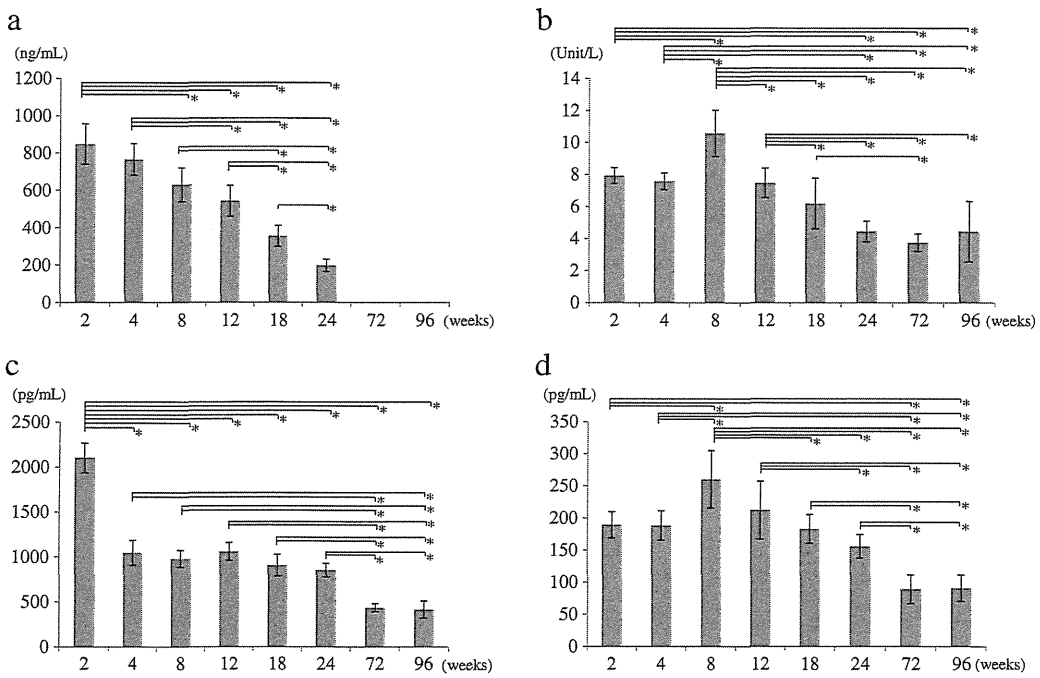

Fig. 5. Plasma levels of other biochemical markers. Plasma levels of the other biochemical markers were evaluated in 2- (n = 5), 4- (n = 5), 8- (n = 6), 12- (n = 6), 18- (n = 6), 24- (n = 5), 72- (n = 5), and 96- (n = 5) week-old male Wistar rats. Values are expressed as means ± SD of plasma levels of the indicated biochemical markers at each age. All comparisons between results from different age groups are shown, with $p < 0.05$ indicating a significant difference (*). (a) Osteocalcin levels. The levels at 72 and 96 weeks were off the register because of the low level of plasma osteocalcin. (b) Trap5b levels. (c) Dkk-1 levels. (d) SOST levels.

Table 5
Correlations between levels of DMP1 and other biochemical markers.

DMP1 levels	vs.	Other bone markers	R	p
DMP1 by ELISA 1–2		DMP1 by ELISA 4–3	0.986	<0.001
DMP1 by ELISA 1–2		TRAP	0.515	<0.001
DMP1 by ELISA 1–2		Osteocalcin	0.800	<0.001
DMP1 by ELISA 1–2		Dkk-1	0.921	<0.001
DMP1 by ELISA 1–2		SOST	0.453	0.002
DMP1 by ELISA 4–3		TRAP	0.512	<0.001
DMP1 by ELISA 4–3		Osteocalcin	0.833	<0.001
DMP1 by ELISA 4–3		Dkk-1	0.910	<0.001
DMP1 by ELISA 4–3		SOST	0.417	0.005

of DMP1, synthesized by osteocytes in the bone, is likely to be released into the blood circulation. Taken together, the novel sandwich ELISAs established with our polyclonal antibodies, which can detect both circulating DMP1 and local bone DMP1, can accurately detect circulating DMP1, which reflects local bone conditions. Further, the results of recovery of recombinant DMP1 and dilution of plasma samples strongly suggested that both ELISA 1–2 and ELISA 4–3 recognized the circulating DMP1 and the standard with similar affinities. The sensitivity of these assays was sufficient to detect circulating DMP1 in healthy male rats of various ages.

Theoretically, ELISAs 1–2 and 4–3 could both detect uncleaved DMP1 as well as the NH_2- and COOH-terminal fragments, respectively. However, protein-chemistry analysis has shown that full-length DMP1 is a precursor that is cleaved into NH_2-terminal 37-kDa and COOH-terminal 57-kDa fragments [4]. Furthermore, it is nearly impossible to detect and extract full-length DMP1 from bone matrix because of the very small quantity of full-length protein in the bone [5]. Indeed, as already noted, ELISAs using pairs of antibodies that recognized uncleaved DMP1 did not have sufficient sensitivity to detect circulating DMP1 (data not shown). Therefore, we conclude that ELISA 1–2 predominantly detects circulating NH_2-terminal fragments of DMP1, and ELISA 4–3 predominantly detects circulating COOH-terminal fragments of DMP1.

Immunoassays using ELISAs 1–2 and 4–3 revealed the same general tendency of reduction in circulating DMP1 levels as a function of age, but there were some differences in measurements obtained using the two ELISAs. The mean values for circulating COOH-terminal DMP1 during rapid skeletal growth (2–12 weeks) were over three times higher than those of circulating NH_2-terminal DMP1. On the other hands, the means of the COOH-terminal and NH_2-terminal DMP1 in samples from older animals (72 and 96 weeks) were almost the same between the two ELISAs. These findings indicated that higher levels of COOH-terminal DMP1 are released from bone tissue during increased production of bone matrix (2–12 weeks), probably due to a difference between the properties of the COOH-terminal and NH_2-terminal fragments. Biochemical studies have shown that NH_2-terminal DMP1 exists as a proteoglycan [19], whereas COOH-terminal DMP1 is highly phosphorylated [4]. In addition to these differences in biochemical properties, our immunohistochemical studies showed that NH_2-terminal DMP1 detected by antibodies specific for DMP1-1 and -2 was predominantly localized in osteocytes and the surrounding bone matrix, whereas COOH-terminal DMP1 detected by antibodies specific for DMP1-3 and -4 was predominantly localized in the pericanalicular matrix in mineralized bone. Maciejewska et al. [20] also reported differences in dental-tissue distribution of the NH_2- and COOH-terminal fragments: in their study, NH_2-terminal DMP1 was restricted to the non-mineralized regions of the tooth predentin, whereas COOH-terminal DMP1 was restricted to the mineralized tooth dentin. Thus, COOH-terminal DMP1 seems to be distributed in mineralized tissue. These differences in biochemical properties and tissue distribution may be related to the higher level of circulating COOH-terminal DMP1 relative to NH_2-terminal DMP1 during rapid growth, but our study has some limitation to understand it. Functional analyses using genetically engineered mice have shown that proteolytic processing of DMP1 is essential to bone formation and mineralization [21], and that the COOH-terminal DMP1 contains the functional domain that controls osteocyte maturation and bone mineralization [22]. Thus, circulating COOH-terminal DMP1, which can be measured by DMP1 ELISA 4–3, may represent a novel marker for osteocyte maturation and bone mineralization.

To explore the relevance of circulating DMP1 as a marker of bone metabolism, we compared levels of DMP1 and other biochemical markers of bone metabolism. We observed that DMP1 levels had the highest positive correlation with levels of Dkk-1, the second highest positive correlation with levels of osteocalcin, and lower positive correlations with levels of Trap5b and SOST. Because DMP1 levels had a high correlation with levels of osteocalcin (a well-known bone-formation marker) [23] and a lower correlation with levels of Trap5b (a well-known bone resorption marker) [24], DMP1 may be a marker of bone formation rather than bone resorption. Some investigators have suggested that osteocalcin is released during bone resorption because a large fraction of synthesized osteocalcin is incorporated into bone; therefore, osteocalcin is also considered to be a marker of bone turnover that indicates the balance between bone formation and resorption [25]. In comparison with osteocalcin produced by mature osteoblasts on the bone surface [26], DMP1 produced by osteocytes within the bone is even more fully incorporated into the inner bone. Therefore, DMP1 should be also released more specifically during bone resorption. We think that this is why DMP1 levels correlate not only the levels of osteocalcin but also the levels of Trap5b. Second, considering that Dkk-1 and SOST act as osteocyte-derived negative regulators of bone formation via inhibition of the Wnt signaling pathway [27–30], the high correlation between DMP1 and Dkk-1 levels and lower correlation between DMP1 and SOST levels are seemingly contradictory. However, the expression patterns of these proteins are not identical: Dkk-1 is expressed in osteoblasts and osteocytes [27], whereas SOST is expressed exclusively in osteocytes [29]. Thus, it is thought that Dkk-1 distributed in superficial bone is easily released into circulating blood, but that SOST distributed only in the inner portion of bone is not easily released into circulating blood. These differences in expression patterns of Dkk-1 and SOST may cause larger differences in the correlation rates between the levels of each protein pair. Third, the highest correlation between circulating Dkk-1 and DMP1 levels and the second highest correlation between circulating osteocalcin and DMP1 levels were observed in this study. These high correlations between the levels of each protein pair may be due to the similar expression patterns of these proteins. That is, osteocalcin is expressed in highly differentiated osteoblasts [26], Dkk-1 in osteoblasts and osteocytes [27], and DMP1 in immature osteocytes [1]. These proteins are expressed at transitional stage of osteoblast-to-osteocyte and distributed in superficial bone and are easily released from it, and hence the circulating levels of these proteins can show similar dynamic state. In addition, based on these situations, circulating DMP1 may be a marker of immature osteocytes rather than mature osteocytes. Further studies are needed to evaluate the significance of circulating DMP1.

Acknowledgments

This work was partially supported by JSPS KAKENHI (Grant-in-aid for Scientific Research), Grant Number 21390491.

Conflicts of interest

This work was supported by Research Foundation of Asahi Kasei Pharma Corporation. Y. Isogai and T. Kuroda are employees of Asahi Kasei Pharma Corporation. Y. Hagiwara and N. Maruyama are employees of Immuno-Biological Laboratories Co., Ltd.

References

[1] Toyosawa S, Shintani S, Fujiwara T, Ooshima T, Sato A, Ijuhin N, et al. Dentin matrix protein 1 is predominantly expressed in chicken and rat osteocytes but not in osteoblasts. J Bone Miner Res 2001;16:2017–26.

[2] Fisher LW, Torchia DA, Fohr B, Young MF, Fedarko NS. Flexible structures of SIBLING proteins, bone sialoprotein, and osteopontin. Biochem Biophys Res Commun 2001;280:460–5.

[3] George A, Sabsay B, Simonian PA, Veis A. Characterization of a novel dentin matrix acidic phosphoprotein. Implications for induction of biomineralization. J Biol Chem 1993;268:12624–30.

[4] Qin C, Brunn JC, Cook RG, Orkiszewski RS, Malone JP, Veis A, et al. Evidence for the proteolytic processing of dentin matrix protein 1 Identification and characterization of processed fragments and cleavage sites. J Biol Chem 2003;278:34700–8.

[5] Huang B, Maciejewska I, Sun Y, Peng T, Qin D, Lu Y, et al. Identification of full-length dentin matrix protein 1 in dentin and bone. Calcif Tissue Int 2008;82:401–10.

[6] Feng JQ, Ward LM, Liu S, Lu Y, Xie Y, Yuan B, et al. Loss of DMP1 causes rickets and osteomalacia and identifies a role for osteocytes in mineral metabolism. Nat Genet 2006;38:1230–1.

[7] Lorenz-Depiereux B, Bastepe M, Benet-Pagès A, Amyere M, Wagenstaller J, Müller-Barth U, et al. DMP1 mutations in autosomal recessive hypophosphatemia implicate a bone matrix protein in the regulation of phosphate homeostasis. Nat Genet 2006;38:1248–50.

[8] Seibel MJ. Molecular markers of bone turnover: biochemical, technical and analytical aspects. Osteoporos Int 2000;11(Suppl. 6):S18–29.

[9] Bonewald LF. The amazing osteocyte. J Bone Miner Res 2011;26:229–38.

[10] Tatsumi S, Ishii K, Amizuka N, Li M, Kobayashi T, Kohno K, et al. Targeted ablation of osteocytes induces osteoporosis with defective mechanotransduction. Cell Metab 2007;5:464–75.

[11] Robling AG, Niziolek PJ, Baldridge LA, Condon KW, Allen MR, Alam I, et al. Mechanical stimulation of bone in vivo reduces osteocyte expression of Sost/sclerostin. J Biol Chem 2008;283:5866–75.

[12] Qiu S, Rao DS, Palnitkar S, Parfitt AM. Reduced iliac cancellous osteocyte density in patients with osteoporotic vertebral fracture. J Bone Miner Res 2003;18:1657–63.

[13] Vashishth D, Verborgt O, Divine G, Schaffler MB, Fyhrie DP. Decline in osteocyte lacunar density in human cortical bone is associated with accumulation of microcracks with age. Bone 2000;26:375–80.

[14] Schneider P, Meier M, Wepf R, Müller R. Towards quantitative 3D imaging of the osteocyte lacuno-canalicular network. Bone 2010;47:848–58.

[15] Mark MP, Butler WT, Prince CW, Finkelman RD, Ruch JV. Developmental expression of 44-kDa bone phosphoprotein (osteopontin) and bone gamma-carboxyglutamic acid (Gla)-containing protein (osteocalcin) in calcifying tissues of rat. Differentiation 1988;37:123–36.

[16] Ikeda T, Nomura S, Yamaguchi A, Suda T, Yoshiki S. In situ hybridization of bone matrix proteins in undecalcified adult rat bone sections. J Histochem Cytochem 1992;40:1079–88.

[17] Chen J, Shapiro HS, Sodek J. Development expression of bone sialoprotein mRNA in rat mineralized connective tissues. J Bone Miner Res 1992;7:987–97.

[18] Olsen JV, Blagoev B, Gnad F, Macek B, Kumar C, Mortensen P, et al. Global, in vivo, and site-specific phosphorylation dynamics in signaling networks. Cell 2006;127:635–48.

[19] Qin C, Huang B, Wygant JN, McIntyre BW, McDonald CH, Cook RG, et al. A chondroitin sulfate chain attached to the bone dentin matrix protein 1 NH_2-terminal fragment. J Biol Chem 2006;281:8034–40.

[20] Maciejewska I, Cowan C, Svoboda K, Butler WT, D'Souza R, Qin C. The NH_2-terminal and COOH-terminal fragments of dentin matrix protein 1 (DMP1) localize differently in the compartments of dentin and growth plate of bone. J Histochem Cytochem 2009;57:155–66.

[21] Sun Y, Prasad M, Gao T, Wang X, Zhu Q, D'Souza R, et al. Failure to process dentin matrix protein 1 (DMP1) into fragments leads to its loss of function in osteogenesis. J Biol Chem 2010;285:31713–22.

[22] Lu Y, Yuan B, Qin C, Cao Z, Xie Y, Dallas SL, et al. The biological function of DMP-1 in osteocyte maturation is mediated by its 57-kDa COOH-terminal fragment. J Bone Miner Res 2011;26:331–40.

[23] Brown JP, Delmas PD, Malaval L, Edouard C, Chapuy MC, Meunier PJ. Serum bone Gla-protein: a specific marker for bone formation in postmenopausal osteoporosis. Lancet 1984;1:1091–3.

[24] Halleen JM, Hentunen TA, Karp M, Käkönen SM, Pettersson K, Väänänen HK. Characterization of serum tartrate-resistant acid phosphatase and development of a direct two-site immunoassay. J Bone Miner Res 1998;13:683–7.

[25] Ivaska KK, Hentunen TA, Vääräniemi J, Ylipahkala H, Pettersson K, Väänänen HK. Release of intact and fragmented osteocalcin molecules from bone matrix during bone resorption in vitro. J Biol Chem 2004;279:18361–9.

[26] Heersche JN, Reimers SM, Wrana JL, Waye MM, Gupta AK. Changes in expression of alpha 1 type 1 collagen and osteocalcin mRNA in osteoblasts and odontoblasts at different stages of maturity as shown by in situ hybridization. Proc Finn Dent Soc 1992;88(Suppl. 1):173–82.

[27] Li J, Sarosi I, Cattley RC, Pretorius J, Asuncion F, Grisanti M, et al. Dkk1-mediated inhibition of Wnt signaling in bone results in osteopenia. Bone 2006;39:754–66.

[28] MacDonald BT, Joiner DM, Oyserman SM, Sharma P, Goldstein SA, He X, et al. Bone mass is inversely proportional to Dkk1 levels in mice. Bone 2007;41:331–9.

[29] van Bezooijen RL, Roelen BA, Visser A, van der Wee-Pals L, de Wilt E, Karperien M, et al. Sclerostin is an osteocyte-expressed negative regulator of bone formation, but not a classical BMP antagonist. J Exp Med 2004;199:805–14.

[30] Poole KE, van Bezooijen RL, Loveridge N, Hamersma H, Papapoulos SE, Löwik CW, et al. Sclerostin is a delayed secreted product of osteocytes that inhibits bone formation. FASEB J 2005;19:1842–4.

Pediatr Radiol
DOI 10.1007/s00247-013-2805-z

CASE REPORT

Benign prenatal hypophosphatasia: a treatable disease not to be missed

Masaki Matsushita · Hiroshi Kitoh · Toshimi Michigami · Kanako Tachikawa · Naoki Ishiguro

Received: 21 March 2013 / Revised: 30 May 2013 / Accepted: 15 September 2013

Abstract Prenatal bowing of the long bones is often associated with severe bone dysplasias. We report a child who presented marked bowing of the long bones at birth but showed a relatively benign postnatal course with spontaneous improvement of bowing. The fetal imaging showed normal skeletal mineralization and normal chest and abdominal circumferences despite the limb bowing and shortening. Decreased serum alkaline phosphatase activity and elevated urine phosphoethanolamine was biochemically evident, and compound heterozygous mutations in the tissue-nonspecific alkaline phosphatase (TNSALP) gene were identified, which confirmed the diagnosis of a benign form of prenatal hypophosphatasia. Benign prenatal hypophosphatasia should be considered in the differential diagnosis of congenital bowing of the long bones.

Keywords Benign prenatal hypophosphatasia · Congenital bowing of the long bones · Tissue-nonspecific alkaline phosphatase

Introduction

Prenatal bowing of the long bones occurs in a number of severe bone dysplasias, including osteogenesis imperfecta, campomelic dysplasia, thanatophoric dysplasia and hypophosphatasia. Hypophosphatasia is a rare inherited disorder caused by deactivating mutations within the gene that encodes the tissue nonspecific isoenzyme of alkaline phosphatase (TNSALP). Inorganic pyrophosphate (PPi), a TNSALP substrate and inhibitor of mineralization, accumulates extracellularly, causing rickets or osteomalacia [1]. Traditionally, hypophosphatasia has been classified as being in prenatal, infantile, childhood and adult forms. Those with dental manifestations but no apparent skeletal disease have been called odontohypophosphatasia [2]. The prenatal or infantile forms are often lethal but enzyme-replacement therapy could improve these life-threatening hypophosphatasias [3]. In 1999, Pauli et al. [4] reported four patients who showed intrauterine deformity but had a benign postnatal course. These patients were diagnosed with benign prenatal hypophosphatasia or "Bent but not broken" hypophosphatasia. More than 200 different defects have been identified in TNSALP [5] and these can be autosomal recessive or autosomal dominant inheritance, which helps to explain the extreme range of severity of the disease. Here we describe a boy who presented prenatal bowing of the long bones suggestive of a severe dysplasia but showed favorable postnatal development. Molecular and biochemical analyses confirmed the diagnosis of the sixth form of hypophosphatasia, a benign prenatal hypophosphatasia.

Case report

The boy was the second child of non-consanguineous healthy parents (Table 1). Screening US in the second trimester was thought to show femoral shortness and bowing, thus the mother was referred to our hospital for further assessment. The femoral lengths at 28 weeks and 36 weeks of gestation were 28.1 mm (−8 SD) and 49 mm (−5.8 SD), respectively. But there was no evidence of abnormalities in chest size, abdominal circumference and bone mineralization.

The infant was delivered at 37 weeks of gestation with birth weight of 2,580 g (−1 SD), length of 41.5 cm (−3.5 SD) and head circumference of 32.5 cm (−1 SD). Apgar scores were 8 and 9 at 1 and 5 min, respectively. Shortening and bowing of

None of the authors received financial support for this study.

M. Matsushita · H. Kitoh (✉) · N. Ishiguro
Department of Orthopaedic Surgery,
Nagoya University Graduate School of Medicine,
65 Tsurumai, Showa-ku, Nagoya,
Aichi 466-8550, Japan
e-mail: hkitoh@med.nagoya-u.ac.jp

T. Michigami · K. Tachikawa
Department of Bone and Mineral Research, Osaka Medical Center
and Research Institute for Maternal and Child Health, Osaka, Japan

Published online: 22 October 2013

Table 1 Patients' summaries

	Original case	Second case
Prenatal ultrasound	Femoral shortness and bowing	Femoral shortness
Condition at birth		
Gestational age (weeks)	37	38
Length (cm)	41.5 (−3.5SD)	43.7 (−2.5SD)
Weight (g)	2,580 (−1SD)	3,020 (0SD)
Head circumference (cm)	32.5 (−1SD)	33.7 (−0.5SD)
Radiographs at neonatal period		
Rickets	–	–
Bowing	Femurs, tibias, fibulas, humeris	Femurs, radius, ulnas
Short femurs	+	+
Bowdler spur	Bilateral fibulae	–
Extremity skin dimples	+	+
Other clinical concerns	Bilateral clubfeet	–
Delayed developing tooth	Not mentioned	+
Tentative diagnosis	Kyphomelic dysplasia	Caffey disease
Age hypophosphatasia diagnosed (years)	4	1
Biochemical data at diagnosis of hypophosphatasia		
Serum ALP IU/L	139	254
Urinary PEA μmol/day	1,417.4	900.8
TNSALP mutation	p.F327L, c.1559delT	p.R30X, p.F327L
Last evaluation		
Age (years)	5	2
Height (SD)	−1.5	−2
Bowing improvement	++	+

HPP Hypophosphatasia, *ALP* Alkaline phosphatase, *PEA* Phosphoethanolamine, *TNSALP* tissue-nonspecific isoenzyme of alkaline phosphatase, *SD* Standard deviation

the upper and lower limbs, skin dimples on the right forearm and the right lower leg, and bilateral clubfeet deformities were recognized neonatally. Initial radiographs taken on the day of birth showed severe symmetrical bowing and shortening of the long tubular bones with mild metaphyseal widening, and normal ossification of the long bones, skull, vertebrae and ribs (Fig. 1a). A tentative diagnosis of atypical kyphomelic dysplasia was made on the basis of shortening and bowing of the long bones with metaphyseal involvement.

Retrospective reviews of additional radiographs clearly demonstrated the presence of characteristic bony spurs in bilateral fibulae, which looked like the Bowdler spur (Fig. 1b). Laboratory tests including normal serum calcium of 5.0 mEq/l and phosphorus of 5.6 mg/dl, decreased alkaline phosphatase (ALP) of 139 IU/L, and elevated levels of urine phosphoethanolamine (PEA) of 1,417 micro-mol/mg (upper limit of normal is 44 micro-mol/mg) were suggestive of a diagnosis of hypophosphatasia. Genomic DNA was extracted from peripheral blood leukocytes and sequencing analysis confirmed the compound heterozygous mutations (c.979T>C; p.F327L and c.1559delT) in the TNSALP gene.

Physical evaluations at the age of 5 years demonstrated no evidence of limb bowing. The lineal growth was normal with the child's height of 102.9 cm (−1.5 SD). Bowing of the long bones spontaneously improved and fibular spurs disappeared, although the skin dimples still remained (Fig. 2a, b).

Discussion

The differential diagnosis of long bone bowing in utero includes severe disorders that have very poor outcomes and early lethality such as prenatal hypophosphatasia, osteogenesis imperfecta, thanatophoric dysplasia, achondrogenesis and campomelic dysplasia [6]. Despite the severity of long bone bowing, the radiographic evidence of normal bone ossification, normal chest size and normal scapular configuration could differentiate our case from these severe diseases. The Bowdler spur, a bony spur emanating from the midshaft of the fibula toward a subjacent skin dimple, is considered a specific radiographic indicator of hypophosphatasia [7]. Assay of serum ALP activity, and quantification of two natural substrates of TNSALP that accumulate

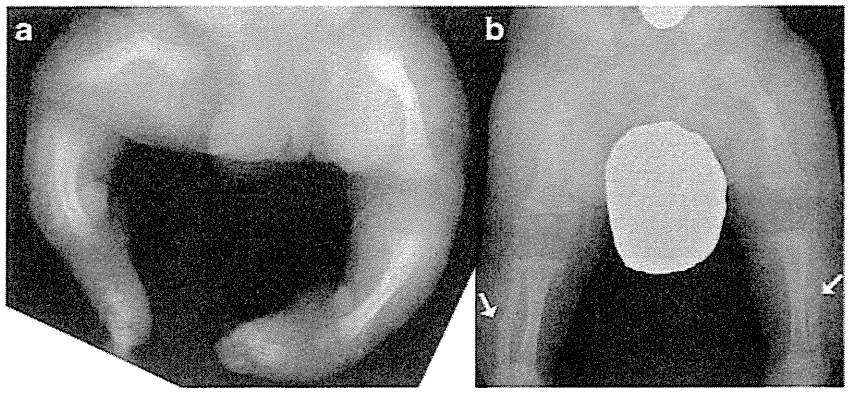

Fig. 1 Anteroposterior radiographs of the lower limbs. **a** A neonatal film shows severe symmetrical bowing and shortening of the long tubular bones with mild metaphyseal widening. **b** A film at the age of 4 months clearly demonstrates bilateral fibular spur (*arrow*)

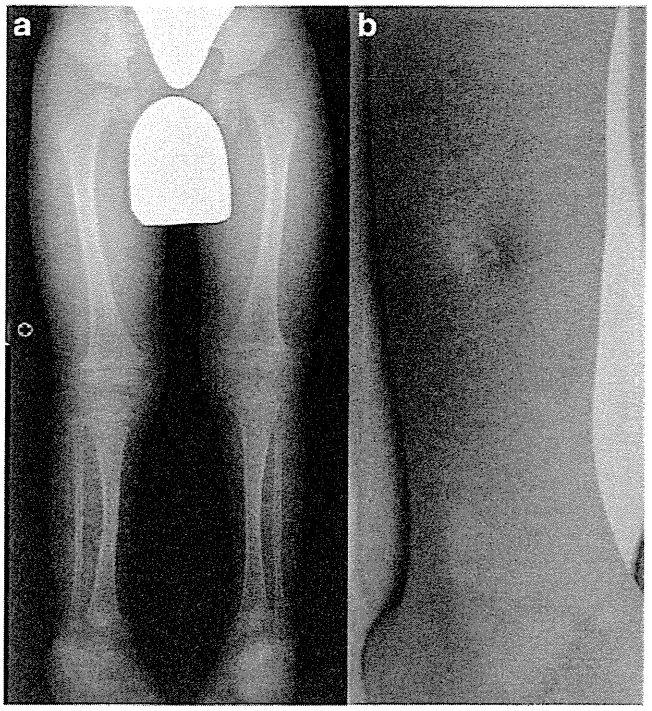

Fig. 2 A 5-year-old boy with prenatal hypophosphatasia. **a** Anteroposterior radiograph of the lower limbs shows improvement of the long bone bowing and disappearance of bilateral fibular spurs. **b** Clinical photo of the right lower limb demonstrates a residual skin dimple

endogenously in hypophosphatasia (pyridoxal 5′-phosphate [PLP] in plasma and PEA in urine) will provide biochemical evidence of hypophosphatasia. Ultimately, definitive diagnosis was made based on molecular testing [8].

Recently, a second boy presented to our institution with benign prenatal hypophosphaatsia (Table 1). The infant was delivered at 38 weeks of gestation with a birth weight of 3,020 g (mean), length of 43.7 cm (−2.5 SD) and head circumference of 33.7 cm (−0.5 SD). Clinical findings at the age of 2 months included shortening and bowing of the thighs and forearms with skin dimples over the site of bilateral forearm angulations. Initial radiographs showed symmetrical bowing and shortening of the femora, radii and ulnae without obvious evidence of fracture or bony spurs (Fig. 3a, b). The humeri, tibiae and fibulae seemed to be normal. The thorax and the vertebral bodies were also normal and the skull was well ossified. He showed normal psychomotor development except for delayed tooth eruption. Laboratory tests revealed low serum ALP of 126 IU/L and elevated levels of urine PEA of 900.8 micro-mol/mg. DNA analysis confirmed the compound heterozygous mutations (c.88C>T; p.R30X and c.979T>C; p.F327L) in the TNSALP gene. Radiographic evaluations at the age of 2.5 years demonstrated persistent but less marked limb shortening and bowing (Fig. 4a, b). The lineal growth was normal with his height of 81 cm (−2 SD).

Mild forms of hypophosphatasia mostly result from heterozygosity for dominant severe alleles or from compound heterozygosity for severe and moderate alleles [8]. Moderate alleles produce significant residual ALP activity, while severe alleles do not usually have enzymatic activity. The F327L mutation has been shown to retain around 70% of enzymatic activity compared with the wild-type protein. On the other hand, c.1559delT mutant identified in the index case, almost completely lost its activity. Michigami et al. [8] reported that patients with F327L mutation in one of the alleles exhibited a relatively mild phenotype despite its prenatal onset, while the c.1559delT mutation was associated with severe forms of hypophosphatasia (prenatal lethal and infantile forms) when not found in patients with the F327L mutation.

Spontaneous improving hypophosphatasia should be added to the list of disorders presenting with prenatal or perinatal bowing of the long bones. We presented several clinical and radiographic characteristics of this specific disease, including congenital bowing and shortening of the long tubular bones that spontaneously improve with time, the Bowdler spur, skin dimples over the site of deformities, tooth abnormalities, and normal ossification of the skull, vertebrae and thorax. Characteristic fetal imaging, including normal bone mineralization, normal chest and abdominal size, and improvement of limb bowing late in the second trimester could lead to the diagnosis of benign prenatal hypophosphatasia, which is a treatable disease.

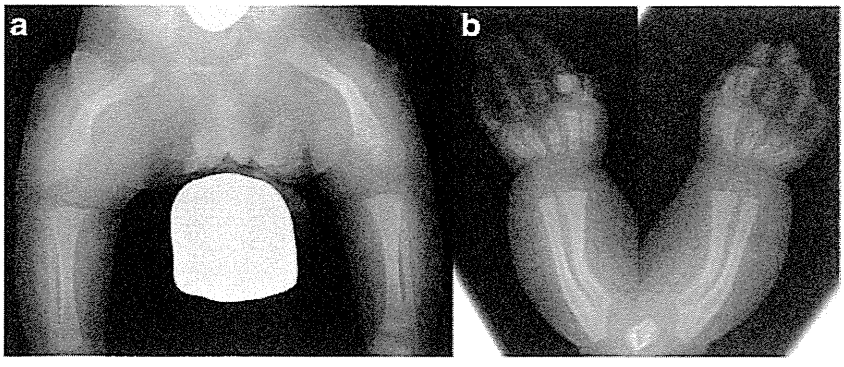

Fig. 3 Anteroposterior radiographs in a 2-month-old boy with prenatal hypophosphatasia. **a** Shortening and bowing of bilateral femora with relatively normal tibiae and fibulae. **b** Marked bowing of the radii and ulnae without evidence of fracture

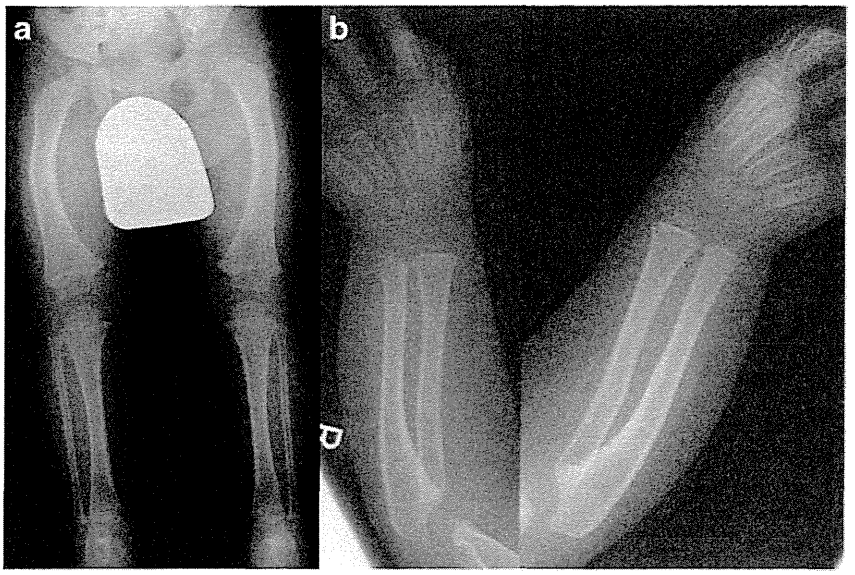

Fig. 4 Anteroposterior radiographs in a 2.5-year-old boy with prenatal hypophosphatasia. **a** Partial improvement of the femoral bowing with cortical thickness at the concave side. **b** Complete healing of the forearm bowing

Conflict of interest The authors declare no conflict of interest.

References

1. Whyte MP (2008) Hypophosphatasia: nature's window on alkaline phosphatase function in humans. In: Bilezikian JP, Raisz LG, Martin TJ (eds) Principles of bone biology, 3rd edn. Academic, San Diego, pp 1573–1598
2. Whyte MP (2012) Hypophosphatasia. In: Glorieux FH, Jueppner H, Pettifor B (eds) Pediatric bone, 2nd edn. Elsevier Academic Press, San Diego, pp 771–794
3. Whyte MP, Greenberg CR, Salman NJ et al (2012) Enzyme-replacement therapy in life-threatening hypophosphatasia. N Engl J Med 366:904–913
4. Pauli RM, Modaff P, Sipes SL et al (1999) Mild hypophosphatasia mimicking severe osteogenesis imperfecta in utero: bent but not broken. Am J Med Genet 86:434–438
5. The Tissue Nonspecific Alkaline Phosphatase Gene Mutation Database. www.sesep.uvsq.fr/03_hypo_mutations.php#mutations. Accessed 9 December 2010
6. Alanay Y, Krakow D, Rimoin DL et al (2007) Angulated femurs and the skeletal dysplasias: experience of the International Skeletal Dysplasia Registry (1988–2006). Am J Med Genet A 143:1159–1168
7. Wenkert D, McAlister WH, Coburn SP et al (2011) Hypophosphatasia: nonlethal disease despite skeletal presentation in utero (17 new cases and literature review). J Bone Miner Res 26:2389–2398
8. Michigami T, Uchihashi T, Suzuki A et al (2005) Common mutations F310L and T1559del in the tissue-nonspecific alkaline phosphatase gene are related to distinct phenotypes in Japanese patients with hypophosphatasia. Eur J Pediatr 164:277–282

Bone 56 (2013) 375–382

Contents lists available at ScienceDirect

Bone

journal homepage: www.elsevier.com/locate/bone

Original Full Length Article

A human skeletal overgrowth mutation increases maximal velocity and blocks desensitization of guanylyl cyclase-B☆

Jerid W. Robinson [a,1], Deborah M. Dickey [b,1], Kohji Miura [c], Toshimi Michigami [d], Keiichi Ozono [c], Lincoln R. Potter [a,b,*]

[a] Department of Pharmacology, University of Minnesota, Minneapolis, MN, USA
[b] Department of Biochemistry, Molecular Biology and Biophysics, University of Minnesota, Minneapolis, MN, USA
[c] Department of Pediatrics, Osaka Graduate School of Medicine, Osaka, Japan
[d] Department of Bone and Mineral Research, Osaka Medical Center and Research Institute for Maternal and Child Health, Osaka, Japan

ARTICLE INFO

Article history:
Received 18 February 2013
Revised 12 June 2013
Accepted 24 June 2013
Available online 1 July 2013

Edited by: R. Baron

Keywords:
Natriuretic peptides
Guanylate cyclase
Bone growth
cGMP
Dwarfism
Achondroplasia

ABSTRACT

C-type natriuretic peptide (CNP) increases long bone growth by stimulating guanylyl cyclase (GC)-B/NPR-B/NPR2. Recently, a Val to Met missense mutation at position 883 in the catalytic domain of GC-B was identified in humans with increased blood cGMP levels that cause abnormally long bones. Here, we determined how this mutation activates GC-B. In the absence of CNP, cGMP levels in cells expressing V883M-GC-B were increased more than 20 fold compared to cells expressing wild-type (WT)-GC-B, and the addition of CNP only further increased cGMP levels 2-fold. In the absence of CNP, maximal enzymatic activity (Vmax) of V883M-GC-B was increased 15-fold compared to WT-GC-B but the affinity of the enzymes for substrate as revealed by the Michaelis constant (Km) was unaffected. Surprisingly, CNP decreased the Km of V883M-GC-B 10-fold in a concentration-dependent manner without increasing Vmax. Unlike the WT enzyme the Km reduction of V883M-GC-B did not require ATP. Unexpectedly, V883M-GC-B, but not WT-GC-B, failed to inactivate with time. Phosphorylation elevated but was not required for the activity increase associated with the mutation because the Val to Met substitution also activated a GC-B mutant lacking all known phosphorylation sites. We conclude that the V883M mutation increases maximal velocity in the absence of CNP, eliminates the requirement for ATP in the CNP-dependent Km reduction, and disrupts the normal inactivation process.

Introduction

C-type natriuretic peptide (CNP) stimulates long bone growth and inhibits meiotic resumption in oocytes by activating the enzyme variously known as guanylyl cyclase (GC)-B, natriuretic peptide receptor (NPR)-2 or NPR-B, which catalyzes the synthesis of the intracellular signaling molecule, cGMP [1–3]. GC-B is a homodimer containing an extracellular ligand-binding domain, a single membrane-spanning region, and an intracellular highly phosphorylated kinase homology domain, dimerization domain and C-terminal GC catalytic domain [4].

CNP binding increases GC-B activity by two mechanisms. It increases the maximal rate of cGMP production called maximal velocity (Vmax) and it also increases the affinity of the enzyme for GTP that is observed as a reduction in the Michaelis constant — the GTP concentration required to reach half the Vmax. Under non-physiologic conditions such as an enzyme assay where ATP is not present, the activity of GC-B is positive cooperative as demonstrated by a Hill coefficient of greater than 1. This means that GTP binds an allosteric site that increases the affinity of the catalytic site for GTP. However, under biological conditions where ATP concentrations are at or above 1 mM, the Hill coefficient of GC-B is 1 because the allosteric site is occupied by ATP not GTP. Recently, we demonstrated that ATP is required for the CNP-dependent reduction in the Km of GC-B [5,6]. Finally, in broken cell assays, ATP also increases GC-B activity by providing the phosphate that is added to the serine and threonine residues on the enzyme that is necessary for activation by CNP [7,8].

GC-B was identified in rat chondrocytes in 1994 [9], but the ability of natriuretic peptides to stimulate skeletal growth was first observed in transgenic mice overexpressing BNP in 1998 [10]. Subsequent bone culture studies indicated that CNP, not BNP, increased the proliferative and hypertrophic zones of the murine growth plate, which increases the length of long bones [10]. CNP also increases the earliest stage of endochondral bone development – the condensation of mesenchymal precursor cells – as well as stimulates glycosaminoglycan synthesis and extracellular matrix production [11,12]. Consistent with the requirement of CNP and GC-B in normal long bone growth in mammals, mice lacking either CNP or GC-B were dwarfs [13,14], and mice lacking the

Abbreviations: CNP, C-type natriuretic peptide; GC, guanylyl cyclase; NP, natriuretic peptide; WT, wild type.

☆ Disclosure statement: The authors have nothing to declare.

* Corresponding author at: University of Minnesota — Twin Cities, 6-155 Jackson Hall, 321 Church St. SE, Minneapolis, MN 55455, USA. Fax: +1 612 624 7282.
E-mail address: potter@umn.edu (L.R. Potter).

[1] Contributed equally to this manuscript and should be considered co-first authors.

8756-3282/$ – see front matter © 2013 Elsevier Inc. All rights reserved.
http://dx.doi.org/10.1016/j.bone.2013.06.024

natriuretic peptide clearance receptor (NPR-C) that degrades CNP exhibited skeletal hyperplasia [15,16]. In contrast, mice lacking BNP display no skeletal abnormalities [17]. Importantly, CNP and CNP analogs were recently shown to increase long bone growth in murine models of achondroplasia [18–20].

Homozygous inactivating mutations in both alleles of GC-B were identified in humans with acromesomelic dysplasia, type Maroteaux (AMDM) dwarfism [21–23], and heterozygous mutations in GC-B were associated with non-pathological reductions in human stature [24]. Conversely, mutations associated with CNP overexpression were identified in patients with skeletal overgrowth [25,26], and a genome-wide association study identified correlations between genetic mutations that regulate CNP or NPR-C expression and height in Northwestern European populations [27].

In 2012, Miura et al. identified a conserved valine to methionine missense mutation at position 883 in the catalytic domain of human GC-B (V883M-GC-B) in three generations of a Japanese family with skeletal overgrowth, fragile bones and elevated blood cGMP concentrations [28]. Importantly, how this mutation increases GC-B activity was not determined. Here, we show that this single residue substitution increases the maximal velocity of GC-B in the absence of CNP and that CNP reduces the Km of V883M-GC-B an order of magnitude without ATP or without increasing maximal velocity. Unexpectedly, the V883M substitution blocked the normal inactivation process.

Materials and methods

Reagents

^{125}I-cGMP radioimmunoassay kits and ^{32}P-α-GTP were from Perkin Elmer (Waltham, MA). CNP-22 was purchased from Sigma (St. Louis, MO). The plasmids encoding the N-terminally HA-tagged form of WT human GC-B (HA-WT-GC-B) [22] and HA-V883M-GC-B plasmids [28] have been described. The plasmids expressing rat GC-B-7A and GC-B-7E were also previously described [29,30]. The ATDC5 chondrocytes were from ATCC (www.atcc.org).

Cells and transfections

293 neocells were maintained and transiently transfected by the HEPES–calcium-phosphate precipitation method as previously reported [30].

Whole cell cGMP elevation assays

Cyclic GMP concentrations were measured by radioimmunoassay in ethanol extracts of transiently transfected 293 cells that were pre-incubated with 1 mM isobutylmethyl xanthine, a general phosphodiesterase inhibitor, for 10 min before being incubated with increasing concentrations of CNP as previously described [31].

Guanylyl cyclase assays

Crude membranes were prepared at 4 °C in phosphatase inhibitor buffer consisting of 50 mM 4-(2-hydroxyethyl)-1-piperazineethanesulfonic acid — pH 7.4, 50 mM NaCl, 20% glycerol, 50 mM NaF, 1 mM EDTA, 0.5 μM microcystin and 1× Roche protease inhibitor cocktail. All assays were performed at 37 °C in a cocktail containing 25 mM HEPES pH 7.4, 50 mM NaCl, 0.1% BSA, 0.5 mM isobutylmethyl xanthine, 1 mM EDTA, 0.5 μM microcystin, 5 mM phosphocreatine, 0.1 μg/μl creatine kinase and 5 mM $MgCl_2$.

The single substrate concentration GC assays were performed using ^{32}P-GTP as substrate in the presence of 1 mM ATP and 1 mM GTP at 37 °C for 3 min as previously described [31]. For the desensitization assays, the reaction was performed using a pool of crude membranes. The reaction was initiated by the addition of pre-warmed cocktail. At the designated times, 0.1 ml aliquots were removed and added to ice-cold tubes containing 0.5 ml zinc acetate to stop the reaction. Alumina column chromatography purified the ^{32}P-cGMP, which was quantified by Cerenkov counting [32].

Substrate-velocity assays were performed for the indicated times with the indicated GTP concentrations. The resulting cGMP concentrations were determined by radioimmunoassay as described [33]. When included, free manganese concentrations in the assays were 2 mM. Because enzymatic activity was not completely linear with time, the kinetic parameters obtained under these conditions are considered "apparent".

Western blotting

293T cells were transfected with the indicated constructs, immunoprecipitated, fractionated by reducing SDS-PAGE and blotted to an Immobilon membrane for immune-detection as previously described [34]. The blot was blocked and probed with at 1/2500 dilution of rabbit serum 6328 followed by incubation with a 1/20,000 dilution of goat anti-rabbit IRDye 680 conjugated antibody and visualized on a LI-COR instrument as previously described [35].

Statistical analysis

Statistics and graphs were generated with Prism 5 software. Student's paired *t*-test determined significance where $p \leq 0.05$ was considered significant. The vertical bars within the symbols represent the SEM. Where not visible the bars are contained within the symbol. EC_{50} values were calculated based on the nonlinear curve fitting equation $Y = Top * X / (EC_{50} + X)$. Substrate–velocity curves were analyzed using an allosteric sigmoidal model to generate Hill coefficients.

Results

Cyclic GMP is elevated more than twenty-fold in cells expressing GC-B-V883M

HEK293 cells were transiently transfected with human isoforms of HA-WT-GC-B or HA-V883M-GC-B. Two days later, the cells were incubated in the presence of increasing concentrations of CNP for 3 min and intracellular cGMP concentrations were determined (Fig. 1A). Basal (no CNP) cGMP concentrations were elevated 21-fold in cells expressing HA-V883M-GC-B compared to cells expressing HA-WT-GC-B. Maximal concentrations of CNP increased cGMP concentrations 29-fold in HA-WT-GC-B expressing cells but only 2-fold in cells expressing HA-V883M-GC-B. The EC_{50} for CNP activation was not significantly different between the WT and mutant enzymes, consistent with the mutation not affecting the affinity of CNP for GC-B.

Plasmids expressing WT and GC-B-V883M were also transiently transfected into ATDC5 mouse chondrocytic cells that endogenously express GC-B. Since these cells express phosphodiesterases 1 and 5, we pretreated them with a general phosphodiesterase to emphasize cGMP synthesis by GC-B [36]. Overexpression of WT-GC-B slightly elevated cyclic GMP concentrations in the ATDC5 cells, but overexpression of the GC-B-V883M mutant resulted in cGMP levels that were more than four-fold higher than those observed in cells transfected with the WT enzyme (Fig. 1B). These data indicate that the increased basal activity associated with the V883M mutation occurs in a natural cellular environment for GC-B and is consistent with the increased plasma cGMP concentrations measured in patients expressing V883M-GC-B [28].

Basal enzymatic activity of V883M-GC-B is elevated but expression is reduced

GC activity was measured in crude membranes from 293 cells expressing green fluorescent protein (GFP) as a control, WT-GC-B,

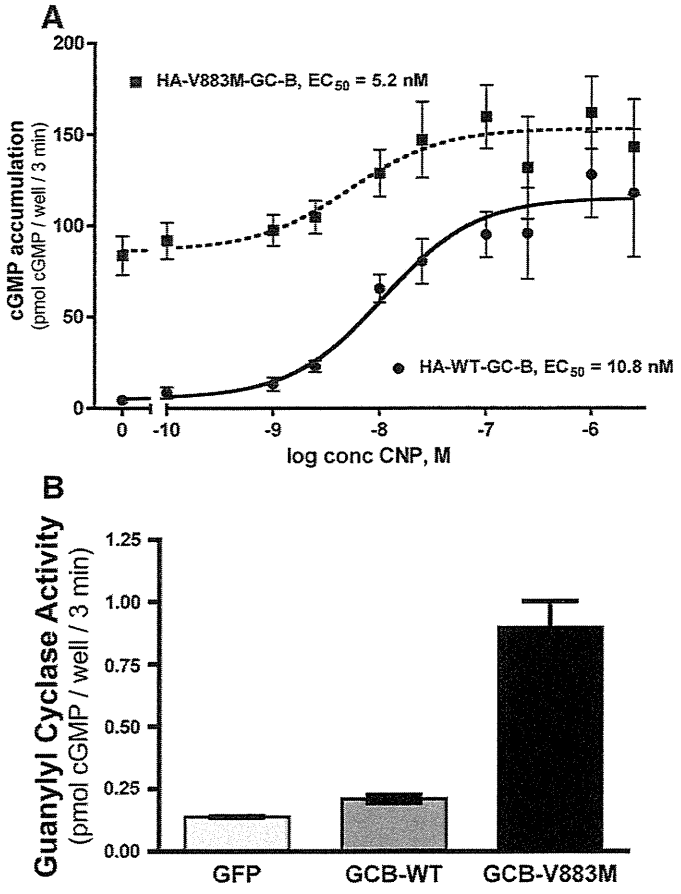

Fig. 1. Basal cGMP concentrations are markedly elevated in cells expressing V883M-GC-B. A, 293 cells transiently expressing HA-WT-GC-B or HA-V883M-GC-B were incubated with the indicated concentrations of CNP for 3 min and then intracellular cGMP concentrations were determined. The EC_{50}s for the two enzymes were not significantly different, $p = 0.42$. B, ATDC5 cells were transiently transfected with plasmids expressing WT-GC-B or GC-B-V883M and cGMP concentrations were measured in basal (no CNP) serum-starved cells 2 days later. Cyclic GMP concentrations in cells expressing WT-GC-B were slightly higher than those observed in un-transfected cells ($p < 0.01$), but levels in cells expressing GC-B-V883M were 4.3-fold higher than those in cells expressing WT-GC-B ($p < 0.03$).

HA-WT-GC-B or HA-V883M-GC-B under basal (1 mM Mg^{2+}GTP), hormone-stimulated (1 mM Mg^{2+}GTP, 1 mM ATP and 1 μM CNP), or detergent-stimulated (1 mM Mn^{2+}GTP and 1% Triton X-100) condition (Fig. 2). Enzyme analysis was performed in the 293 cells because they do not express detectable endogenous GC activity [6], which allows more definitive interpretation of the data because most tissues and cell lines express more than one GC.

GC activity measured in crude membranes from GFP transfected cells was insignificant under all conditions. Consistent with the whole cell cGMP analysis describe in Fig. 1, basal GC activity was low for WT-GC-B and HA-WT-GC-B but was elevated 28-fold over WT levels for HA-V883M-GC-B. Saturating concentrations of CNP and ATP stimulated WT-GC-B and HA-WT-GC-B similarly (>50-fold). However, GC activity of HA-WT-GC-B was almost double that of the WT enzyme lacking the HA tag, consistent with higher expression of the HA-tagged receptor. As in whole cells, CNP and ATP activated HA-V883M-GC-B about two-fold in enzyme assays. GC activity of HA-V883M-GC-B measured in the presence of detergent was lower than that observed for HA-WT-GC-B, which is consistent with reduced expression of HA-V883M-GC-B compared to HA-WT-GC-B. Western analysis of SDS-PAGE fractionated immunoprecipitated enzymes confirmed that the more slowly migrating, completely processed species (upper band) was expressed at lower levels than the comparably processed forms of the tagged or untagged WT version of GC-B (Fig. 2, inset). We previously

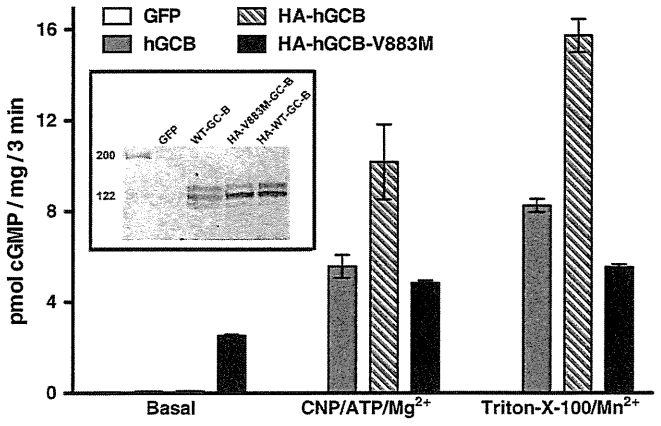

Fig. 2. GC activity but not the protein level of V883M-GC-B was elevated in the absence of CNP. Crude membranes from 293 cells transfected with plasmids expressing the indicated constructs were assayed for GC activity under the conditions indicated in the figure legend and text. Bars within the symbols indicate the range of duplicate determinations. This figure is representative of two independent assays. The inset shows a Western blot of the indicated forms of GC-B purified from 293 cells transiently transfected with the indicated constructs. The numbers on the left indicate the molecular weight of standards.

demonstrated that only the upper band of GC-B is phosphorylated and that phosphorylation is required for CNP-dependent activation of GC-B [8,29].

Maximal velocity of HA-GC-B-V883M is elevated

To determine how the mutation increased the enzymatic activity of GC-B, substrate–velocity curves were generated for HA-WT-GC-B and HA-V883M-GC-B with or without 1 μM CNP in the absence of ATP (Fig. 3A). Basal activity of the WT enzyme was low and CNP increased Vmax 12-fold without decreasing the Km. Consistent with previous observations [6], WT-GC-B was positive cooperative as indicated by a Hill slope of 1.3. In contrast, basal maximal velocity of the mutant enzyme was elevated 15-fold compared to WT-GC-B and the Km was unchanged. The Hill coefficient was 0.9, suggesting slight negative cooperativity. CNP failed to increase the maximal velocity of HA-V883M-GC-B, but reduced the Hill slope 0.4 units and the Km 10-fold. Thus, the V883M mutation increases basal maximal velocity, reduces the Hill coefficient and allows CNP to reduce the Km in the absence of ATP. In contrast, the reduction in Hill coefficient and Km for the WT enzyme was previously shown to be completely dependent on the presence of ATP [5]. These data are consistent with the V883M mutation producing a structural change in GC-B that locks it into a conformation that mimics that of the ATP-bound state. They also indicate for the first time that the CNP-dependent changes in the Vmax and Km of GC-B are separate but related processes.

CNP reduces the Hill coefficient and Km of HA-V883M-GC-B in a concentration-dependent manner in the absence of ATP

Substrate–velocity curves were generated for HA-V883M-GC-B in the presence of increasing concentrations of CNP to evaluate the concentration-dependence of CNP on reductions in the Hill coefficient and Michaelis constant (Fig. 3B). ATP was not included in these experiments. In the absence of CNP, no cooperativity was observed, but increasing concentrations of CNP progressively increased the amount of negative cooperativity while concomitantly decreasing the Km. These data indicate that CNP converts HA-V883M-GC-B to a strongly negative cooperative enzyme. Similarly, in the absence of CNP, the Km of the mutant enzyme was high; but in the presence of increasing concentrations of CNP, the Km dropped progressively while maximal velocity was unaffected.

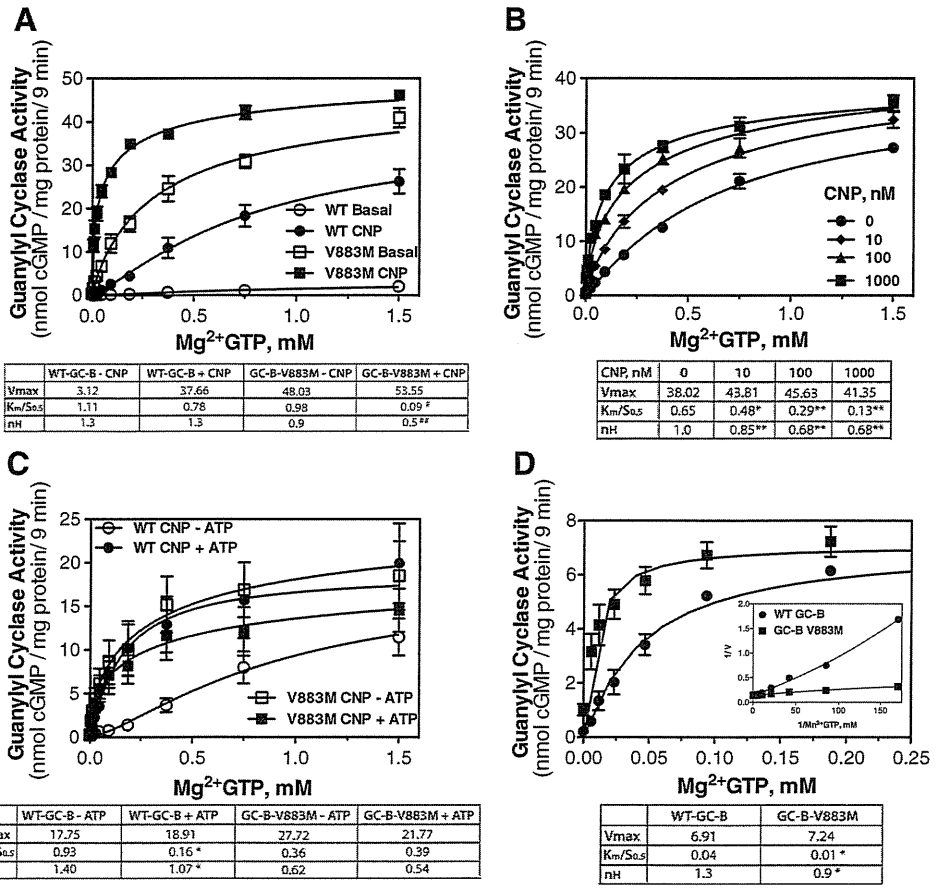

	WT-GC-B - CNP	WT-GC-B + CNP	GC-B-V883M - CNP	GC-B-V883M + CNP
Vmax	3.12	37.66	48.03	53.55
Km/S0.5	1.11	0.78	0.98	0.09 #
nH	1.3	1.3	0.9	0.5 ##

CNP, nM	0	10	100	1000
Vmax	38.02	43.81	45.63	41.35
Km/S0.5	0.65	0.48*	0.29**	0.13**
nH	1.0	0.85**	0.68**	0.68**

	WT-GC-B - ATP	WT-GC-B + ATP	GC-B-V883M - ATP	GC-B-V883M + ATP
Vmax	17.75	18.91	27.72	21.77
Km/S0.5	0.93	0.16 *	0.36	0.39
nH	1.40	1.07 *	0.62	0.54

	WT-GC-B	GC-B-V883M
Vmax	6.91	7.24
Km/S0.5	0.04	0.01 *
nH	1.3	0.9 *

Fig. 3. Kinetic characterization of V883M-GC-B. GC activity shown in panels A–D was measured for 9 min in crude membranes from 293 cells transiently expressing either HA-GC-B-WT or HA-GC-B-V883M. Bars within symbols indicate the SEM. Tables below each figure show Vmax, Km and Hill coefficient (n_H). A. Maximal velocity of HA-V883M-GC-B is elevated in the absence of CNP. GC activity was measured in the presence or absence of 1 μM CNP and the indicated concentrations of Mg^{2+}GTP where n = 4. The # indicates a significant difference from HA-WT-GC-B-CNP at $p < 0.05$. The ## indicates a significant difference from HA-V883M-GC-B-CNP at $p < 0.03$. B. CNP decreases the Hill coefficient and Km for HA-V883M-GC-B in a concentration-dependent manner in the absence of ATP. GC activity was measured in the presence or absence of increasing concentrations of CNP and the indicated concentrations of Mg^{2+}GTP where n = 4. * and ** indicate a significant difference from no CNP values where $p < 0.05$ and 0.01, respectively. C. ATP does not affect the Hill coefficient or Km of HA-V883M-GC-B. GC activity was measured in the presence or absence of 0.1 mM ATP, 1 μM CNP and the indicated concentrations of Mg^{2+}GTP where n = 4. The * indicates a significant difference from HA-WT-GC-B (−) ATP at $p < 0.05$. D. HA-V883M-GC-B is negative cooperative. GC activity was measured with the indicated concentrations of Mn^{2+}GTP and 1% Triton X-100 where n = 6. The * indicates a significant difference from the corresponding value obtained for the WT enzyme at $p < 0.05$; inset. Double reciprocal plots were generated from the raw data to demonstrate a concave upward curve indicative of positive cooperativity or a slightly downward curve indicative of negative cooperativity.

ATP does not allosterically activate V883M-GC-B

We recently determined that CNP reduces the Hill coefficient and Km of WT-GC-B by a process that requires ATP binding to an allosteric site in the catalytic domain [6]. Therefore, we investigated whether the V883M mutation affected these processes as well. Substrate–velocity curves were generated for HA-WT-GC-B and HA-V883M-GC-B in the presence of 1 μM CNP with or without 0.1 mM ATP. With the WT enzyme, ATP reduced the Km 6-fold and the Hill coefficient 0.3 units without affecting the Vmax (Fig. 3C). However, ATP failed to reduce the Km or Hill coefficient or increase the Vmax of HA-V883M-GC-B. These data are consistent with a scenario where the V883M mutation causes a conformational change in GC-B that abolishes the need for ATP in the CNP-dependent reduction in Hill coefficient and Km.

HA-V883M-GC-B is slightly negative cooperative when manganese is used as a cofactor

Substrate–velocity curves were also generated on membranes expressing HA-WT-GC-B or HA-V883M-GC-B under non-physiologic, detergent conditions using manganese-GTP as substrate (Fig. 3D). Substrate–velocity curves generated under these conditions were previously shown to be positive cooperative for GC-A [37]. Vmax was lower when measured under these conditions but the Km/S0.5 was strikingly lower compared to physiologic activation conditions. Maximal velocity was not different between the WT and mutant GC-B enzymes. The substrate–velocity curve for HA-WT-GC-B was positive cooperative as demonstrated by concave upward reciprocal plots and a Hill coefficient of 1.3 (Fig. 3D, inset). To our knowledge, this is the first demonstration of positive cooperativity for GC-B when assayed under detergent-stimulated conditions. In contrast to HA-WT-GC-B, HA-V883M-GC-B was weakly negative cooperative as indicated by a slightly concave downward curve and a Hill coefficient of 0.9 (Fig. 3D, inset), which is consistent with the slight negative cooperativity observed for V883-GC-B when assayed under basal conditions.

HA-V883M-GC-B is resistant to desensitization

Cyclic GMP concentrations in cells expressing V883M-GC-B were highly elevated two days after transfection (Fig. 1), which suggests that the mutant enzyme was not completely desensitized or downregulated. In contrast, CNP activated WT-GC-B was shown to desensitize in less than one hour [8]. Therefore, we examined whether the V883M mutation disrupted the inactivation of GC-B.

GC activity was measured on membranes from cells expressing HA-WT-GC-B or HA-V883M-GC-B for up to 2 h to evaluate the effect of the V883M mutation on the inactivation of GC-B as a function of time (Fig. 4, top panel). WT GC activity was determined in the

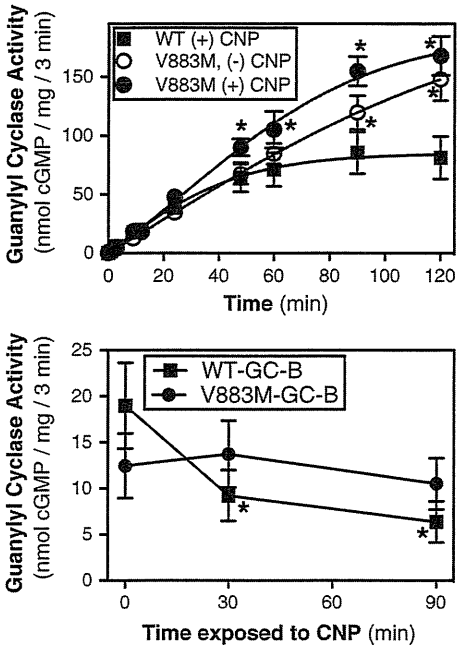

Fig. 4. V883M-GC-B is resistant to desensitization. A. GC assays were conducted on crude membranes from 293 cells transfected with HA-WT-GC-B or HA-V883M-GC-B for the period of time indicated in the presence of 1 mM GTP, 1 mM ATP and 5 mM $Mg^{2+}Cl_2$ with or without 1 μM CNP. Each value represents 4 determinations. The asterisks indicate a significant difference from corresponding values obtained in membranes expressing WT-GC-B at $p < 0.02$. B. Whole 293 cells transfected with HA-WT-GC-B or HA-V883M-GC-B were incubated with 1 μM CNP for the indicated times. Membranes were then prepared and assayed for GC activity in the presence of 1 mM GTP, 1 mM ATP and 5 mM $Mg^{2+}Cl_2$. N = 4. The asterisks indicate significance from the 0 time point value where $p < 0.05$. The bars within the symbols indicate SEM in all panels.

presence of CNP, whereas mutant activity was determined in the presence and absence of CNP. The GC activity of the WT enzyme declined with time and was inactive after 60 min. In contrast, the GC activity of the mutant receptor was linear for the duration of the assay regardless of whether CNP was included in the assay.

We also examined the inactivation of the WT and mutant enzymes under whole cell conditions. In this experiment, intact cells were treated with 1 μM CNP for 0, 30 or 90 min then membranes were prepared from the cells and assayed for GC activity for 3 min (Fig. 4, bottom panel). The WT enzyme demonstrated a time-dependent inactivation similar to that previously reported for GC-B expressed in 3T3 cells [8]. However, exposure of the V883M-GC-B to saturating concentrations of CNP failed to inactivate the enzyme after 30 or 90 min. Together, these data indicate that the Val substitution at position 883 not only increases the maximal velocity of the enzyme, it also disrupts the normal desensitization process.

Activation of GC-B by the V883M substitution does not require phosphorylation

CNP only activated a GC-B construct containing alanine substitutions for the first six phosphorylation sites identified in GC-B (S513, T516, S518, S523, S526, T529) two-fold as opposed to greater than 30-fold for WT-GC-B [29], whereas the analogous substitutions left GC-A completely unresponsive to NP stimulation [38]. These observations led to the idea that phosphorylation is required for NP-dependent activation of GC-A and GC-B. Here, we asked whether phosphorylation is also required for the V883M mutation to increase GC-B activity.

To do this, we mutated Val-883 to Met in the rat GC-B-7A construct that contains alanine substitutions for the first six identified sites plus Ser-522, which is not phosphorylated [29]. We also created a constitutively phosphorylated mimetic version of rat GC-B-V883M by mutating Val-883 to Met in GC-B-7E. Rat GC-B-7E contains glutamate substitutions for the first six identified sites as well as Ser-489, a newly identified putative site that reduces the Km of GC-B when phosphorylated [30].

Introducing the Val-883–Met mutation into WT-GC-B increased basal activity 39-fold, whereas the same mutation in the dephosphorylated form of the enzyme (GC-B-7A) increased activity 17-fold (Fig. 5). However, introduction of the V883M mutation into the GC-B-7E construct increased activity 68-fold. Thus, phosphorylation is not required for the elevated basal activity associated with the V883M mutation, but phosphorylation results in greater activation since the WT and phosphorylation mimetic enzymes (GC-B-7E) were activated to a greater degree than the non-phosphorylated enzyme (GC-B-7A).

Discussion

Characterization of the missense mutant revealed several important changes in GC-B that occurred as a result of this single amino acid substitution. First, basal maximal velocity was dramatically increased. Second, the CNP-dependent reduction in Km was rendered independent of ATP, and thirdly, the normal desensitization process was inactivated. Another worthy point of discussion is that the V883M-GC-B mutant is the first example of a GC where ligand binding reduces the Km without increasing maximal velocity. Thus, the kinetic analysis of this mutant allowed the separation of the maximal velocity increasing effects of ligand binding from the Km reducing effects of ligand binding for the first time. This mutant enzyme also provides unequivocal support for the new GC-B activation model where CNP binding increases activity by reducing the Km as well as increasing maximal velocity [6].

Early studies indicated that product formation by membrane GCs in the presence of detergent is positive cooperative [39,40]. We found that GC-B is positive cooperative under basal conditions as well as when assayed in the presence of Mn^{2+}GTP and Triton X-100. However, the single V883M mutation converts the enzyme from positive cooperative to slightly negative cooperative when assayed under both physiologic and detergent-activated conditions. Interestingly, CNP increased the degree of negative cooperativity of V883M-GC-B in a concentration-dependent manner.

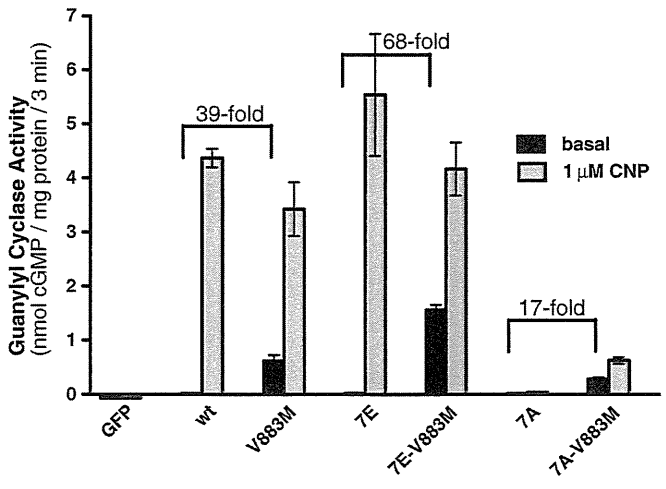

Fig. 5. The GC-B-V883M mutation activates a dephosphorylated version of GC-B. The V883M mutation was introduced into WT-GC-B, constitutively phosphorylated (7E) or constitutively dephosphorylated (7A) forms of GC-B. 293 cells were transiently transfected with plasmids expressing the indicated GC-B constructs. GC assays were performed for 3 min in the presence of 0.1 mM GTP, 1 mM ATP and 5 mM $Mg^{2+}Cl_2$ with or without 1 μM CNP. Each value represents 6 determinations. The bars within the symbols indicate SEM. The values above the brackets indicate the fold-difference above basal values.

The reduction in Km and increase in negative cooperativity appear paradoxical. We hypothesize that the V883M mutant locks the enzyme into a conformation that mimics an ATP bound state. This hypothesis is supported by low or no cooperativity under basal conditions and the inability of ATP to change the activity of the mutant enzyme. In addition, CNP alone markedly decreased the Km of GC-B-V883M, a phenomenon that requires ATP with the WT enzyme. Since cooperativity is maintained, this suggests that the mutation does not destroy the ability of GTP to bind to the allosteric site but rather modifies how GTP binding to the allosteric site affects the catalytic site. However, an alternative

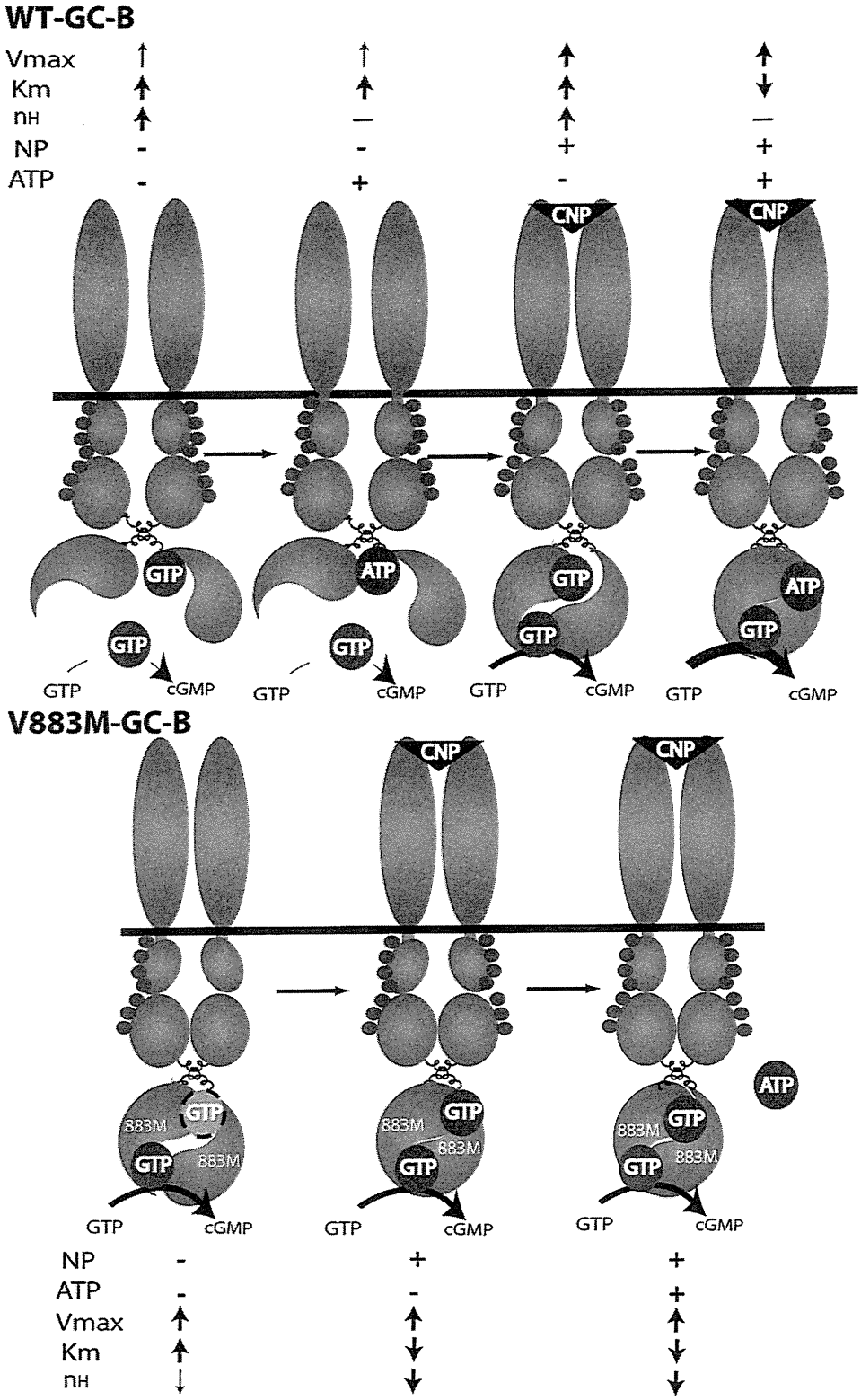

Fig. 6. Activation models for wild type and mutant GC-B. The models are described in detail under the Discussion section. The blue spheres indicate known phosphorylation sites in the kinase homology domain of GC-B. The white 883M indicates that the Val to Met mutation is in the catalytic domain. The abbreviations are: CNP, C-type natriuretic peptide; Km, Michaelis constant; n_H, Hill coefficient; and Vmax, maximal velocity.

explanation is that the reduction in the Hill coefficient results from increased inhibition resulting from GTP binding to a site independent of the allosteric site. This third GTP binding site would explain the appearance of negative cooperativity while also allowing for the Km reduction resulting from the previously identified allosteric site. It is also possible that the V883M mutation could increase the affinity of GC-B for the products of the reaction (pyrophosphate and cGMP), which would result in reduced GC activity and apparent negative cooperativity. Importantly, since the V883M mutation did not affect Vmax when measured in the presence of detergent and manganese, it suggests that the mutation modifies the conformation of the active site under physiologic conditions and does not directly interact with the substrate.

Near linear cGMP production with time by HA-V883M-GC-B assayed both in the presence and absence of CNP indicated that HA-V883M-GC-B is resistant to desensitization. Experiments with alanine and glutamate substituted receptors indicated that unlike CNP activation of WT-GC-B, the increased activity observed with the V883M mutation does not require phosphorylation of the kinase homology domain, although activation was greater with the phosphorylated and phosphomimetic enzymes. The lack of dependence on phosphorylation for activity of the mutant enzyme may contribute to its resistance to desensitization.

It is surprising how much the single amino acid substitution changes the regulation of GC-B (Fig. 6). In the absence of CNP and ATP, maximal velocity of WT-GC-B was low, affinity for substrate was low (high Km), and cooperative was significant and positive. In contrast, under the same conditions, maximal velocity of V883M-GC-B was high, affinity for substrate was low, and cooperativity was low and negative. Addition of ATP in the absence of CNP abolished positive cooperativity of the WT enzyme due to ATP replacing GTP at the allosteric site [6], but had no effect on the mutant enzyme under identical conditions. CNP alone increased maximal velocity of the WT enzyme, but it did not decrease the Km in the absence of ATP. In contrast, CNP alone failed to increase maximal velocity of the mutant enzyme but decreased the Km ten-fold in the absence of ATP. Finally, CNP reduced the cooperativity of both enzymes, but the WT enzyme went from positive to no cooperativity, whereas the mutant went from slightly negative cooperative to very negative cooperative.

In conclusion, we established a molecular mechanism for how a single amino acid substitution in GC-B activates the enzyme, which results in abnormally long and fragile human bones. It will be interesting to determine the prevalence of this mutation in humans and other species.

Conflict of interest statement

None of the authors have a conflict of interest associated with this study.

Acknowledgments

Grant-in Aid (21,922) from the University of Minnesota Graduate School to LRP and the National Institute of Arthritis and Musculoskeletal and Skin Diseases Training Grant T32AR050938 to JWR supported this work.

References

[1] Tamura N, Doolittle LK, Hammer RE, Shelton JM, Richardson JA, Garbers DL. Critical roles of the guanylyl cyclase B receptor in endochondral ossification and development of female reproductive organs. Proc Natl Acad Sci U S A 2004;101:17300–5.
[2] Schmidt H, Stonkute A, Juttner R, Schaffer S, Buttgereit J, Feil R, et al. The receptor guanylyl cyclase Npr2 is essential for sensory axon bifurcation within the spinal cord. J Cell Biol 2007;179:331–40.
[3] Zhang M, Su YQ, Sugiura K, Xia G, Eppig JJ. Granulosa cell ligand NPPC and its receptor NPR2 maintain meiotic arrest in mouse oocytes. Science 2010;330:366–9.
[4] Potter LR, Hunter T. Guanylyl cyclase-linked natriuretic peptide receptors: structure and regulation. J Biol Chem 2001;276:6057–60.
[5] Antos LK, Potter LR. Adenine nucleotides decrease the apparent Km of endogenous natriuretic peptide receptors for GTP. Am J Physiol Endocrinol Metab 2007;293:E1756–63.
[6] Robinson JW, Potter LR. Guanylyl cyclases A and B are asymmetric dimers that are allosterically activated by ATP binding to the catalytic domain. Sci Signal 2012;5:ra65.
[7] Duda T, Goraczniak RM, Sitaramayya A, Sharma RK. Cloning and expression of an ATP-regulated human retina C-type natriuretic factor receptor guanylate cyclase. Biochemistry 1993;32:1391–5.
[8] Potter LR. Phosphorylation-dependent regulation of the guanylyl cyclase-linked natriuretic peptide receptor B: dephosphorylation is a mechanism of desensitization. Biochemistry 1998;37:2422–9.
[9] Hagiwara H, Sakaguchi H, Itakura M, Yoshimoto T, Furuya M, Tanaka S, et al. Autocrine regulation of rat chondrocyte proliferation by natriuretic peptide C and its receptor, natriuretic peptide receptor-B. J Biol Chem 1994;269:10729–33.
[10] Suda M, Ogawa Y, Tanaka K, Tamura N, Yasoda A, Takigawa T, et al. Skeletal overgrowth in transgenic mice that overexpress brain natriuretic peptide. Proc Natl Acad Sci U S A 1998;95:2337–42.
[11] Krejci P, Masri B, Fontaine V, Mekikian PB, Weis M, Prats H, et al. Interaction of fibroblast growth factor and C-natriuretic peptide signaling in regulation of chondrocyte proliferation and extracellular matrix homeostasis. J Cell Sci 2005;118:5089–100.
[12] Woods A, Khan S, Beier F. C-type natriuretic peptide regulates cellular condensation and glycosaminoglycan synthesis during chondrogenesis. Endocrinology 2007;148:5030–41.
[13] Chusho H, Tamura N, Ogawa Y, Yasoda A, Suda M, Miyazawa T, et al. Dwarfism and early death in mice lacking C-type natriuretic peptide. Proc Natl Acad Sci U S A 2001;98:4016–21.
[14] Tamura N, Garbers DL. Regulation of the guanylyl cyclase-B receptor by alternative splicing. J Biol Chem 2003;278:48880–9.
[15] Jaubert J, Jaubert F, Martin N, Washburn LL, Lee BK, Eicher EM, et al. Three new allelic mouse mutations that cause skeletal overgrowth involve the natriuretic peptide receptor C gene (Npr3). Proc Natl Acad Sci U S A 1999;96:10278–83.
[16] Matsukawa N, Grzesik WJ, Takahashi N, Pandey KN, Pang S, Yamauchi M, et al. The natriuretic peptide clearance receptor locally modulates the physiological effects of the natriuretic peptide system. Proc Natl Acad Sci U S A 1999;96:7403–8.
[17] Tamura N, Ogawa Y, Chusho H, Nakamura K, Nakao K, Suda M, et al. Cardiac fibrosis in mice lacking brain natriuretic peptide. Proc Natl Acad Sci U S A 2000;97:4239–44.
[18] Kake T, Kitamura H, Adachi Y, Yoshioka T, Watanabe T, Matsushita H, et al. Chronically elevated plasma C-type natriuretic peptide level stimulates skeletal growth in transgenic mice. Am J Physiol Endocrinol Metab 2009;297:E1339–48.
[19] Lorget F, Kaci N, Peng J, Benoist-Lasselin C, Mugniery E, Oppeneer T, et al. Evaluation of the therapeutic potential of a CNP analog in a Fgfr3 mouse model recapitulating achondroplasia. Am J Hum Genet 2012;91:1108–14.
[20] Yasoda A, Kitamura H, Fujii T, Kondo E, Murao N, Miura M, et al. Systemic administration of C-type natriuretic peptide as a novel therapeutic strategy for skeletal dysplasias. Endocrinology 2009;150:3138–44.
[21] Bartels CF, Bukulmez H, Padayatti P, Rhee DK, van Ravenswaaij-Arts C, Pauli RM, et al. Mutations in the transmembrane natriuretic peptide receptor NPR-B impair skeletal growth and cause acromesomelic dysplasia, type Maroteaux. Am J Hum Genet 2004;75:27–34.
[22] Hachiya R, Ohashi Y, Kamei Y, Suganami T, Mochizuki H, Mitsui N, et al. Intact kinase homology domain of natriuretic peptide receptor-B is essential for skeletal development. J Clin Endocrinol Metab 2007;92:4009–14.
[23] Khan S, Hussain Ali R, Abbasi S, Nawaz M, Muhammad N, Ahmad W. Novel mutations in natriuretic peptide receptor-2 gene underlie acromesomelic dysplasia, type Maroteaux. BMC Med Genet 2012;13:44.
[24] Olney RC, Bukulmez H, Bartels CF, Prickett TC, Espiner EA, Potter LR, et al. Heterozygous mutations in natriuretic peptide receptor-B (NPR2) are associated with short stature. J Clin Endocrinol Metab 2006;91:1229–32.
[25] Bocciardi R, Ravazzolo R. C-type natriuretic peptide and overgrowth. Endocr Dev 2009;14:61–6.
[26] Moncla A, Missirian C, Cacciagli P, Balzamo E, Legeai-Mallet L, Jouve JL, et al. A cluster of translocation breakpoints in 2q37 is associated with overexpression of NPPC in patients with a similar overgrowth phenotype. Hum Mutat 2007;12:1183–8.
[27] Estrada K, Krawczak M, Schreiber S, van Duijn K, Stolk L, van Meurs JB, et al. A genome-wide association study of northwestern Europeans involves the C-type natriuretic peptide signaling pathway in the etiology of human height variation. Hum Mol Genet 2009;18:3516–24.
[28] Miura K, Namba N, Fujiwara M, Ohata Y, Ishida H, Kitaoka T, et al. An overgrowth disorder associated with excessive production of cGMP due to a gain-of-function mutation of the natriuretic peptide receptor 2 gene. PLoS One 2012;7:e42180.
[29] Potter LR, Hunter T. Identification and characterization of the major phosphorylation sites of the B-type natriuretic peptide receptor. J Biol Chem 1998;273:15533–9.
[30] Yoder AR, Robinson JW, Dickey DM, Andersland J, Rose BA, Stone MD, et al. A functional screen provides evidence for a conserved, regulatory, juxtamembrane phosphorylation site in guanylyl cyclase A and B. PLoS One 2012;7:e36747.
[31] Dickey DM, Burnett Jr JC, Potter LR. Novel bifunctional natriuretic peptides as potential therapeutics. J Biol Chem 2008;283:35003–9.
[32] Bryan PM, Potter LR. The atrial natriuretic peptide receptor (NPR-A/GC-A) is dephosphorylated by distinct microcystin-sensitive and magnesium-dependent protein phosphatases. J Biol Chem 2002;277:16041–7.
[33] Robinson JW, Potter LR. ATP potentiates competitive inhibition of guanylyl cyclase A and B by the staurosporine analog, Go6976: reciprocal regulation of ATP and GTP binding. J Biol Chem 2011;286:33841–4.
[34] Abbey-Hosch SE, Smirnov D, Potter LR. Differential regulation of NPR-B/GC-B by protein kinase C and calcium. Biochem Pharmacol 2005;70:686–94.

[35] Flora DR, Potter LR. Prolonged atrial natriuretic peptide exposure stimulates guanylyl cyclase-A degradation. Endocrinology 2010;151:2769–76.
[36] Fujishige K, Kotera J, Yanaka N, Akatsuka H, Omori K. Alteration of cGMP metabolism during chondrogenic differentiation of chondroprogenitor-like EC cells, ATDC5. Biochim Biophys Acta 1999;1452:219–27.
[37] Ivanova K, Heim JM, Gerzer R. Kinetic characterization of atrial natriuretic factor-sensitive particulate guanylate cyclase. Eur J Pharmacol 1990;189:317–26.
[38] Potter LR, Hunter T. Phosphorylation of the kinase homology domain is essential for activation of the A-type natriuretic peptide receptor. Mol Cell Biol 1998;18: 2164–72.
[39] Chrisman TD, Garbers DL, Parks MA, Hardman JG. Characterization of particulate and soluble guanylate cyclases from rat lung. J Biol Chem 1975;250:374–81.
[40] Kimura H, Murad F. Evidence for two different forms of guanylate cyclase in rat heart. J Biol Chem 1974;249:6910–6.

Razzaque MS (ed): Phosphate and Vitamin D in Chronic Kidney Disease.
Contrib Nephrol. Basel, Karger, 2013, vol 180, pp 14–24 (DOI: 10.1159/000346776)

Extracellular Phosphate as a Signaling Molecule

Toshimi Michigami

Department of Bone and Mineral Research, Osaka Medical Center and Research Institute for Maternal and Child Health, Izumi, Osaka, Japan

Abstract

Phosphorus is involved in various biological processes including membrane integrity, maintenance and inheritance of genetic materials, energy metabolism, intracellular signaling and skeletal mineralization. In addition, accumulating evidences have indicated that alteration in the levels of extracellular inorganic phosphate (Pi) itself triggers signaling to regulate gene expression and cellular functions in some cell types. In bone cells such as osteoblasts and chondrocytes, extracellular Pi modulates cell proliferation, differentiation, mineralization and apoptosis. In extraskeletal tissues, extracellular Pi also exerts various effects. For example, increased extracellular Pi results in the calcification associated with the upregulation of osteoblast marker genes in vascular smooth muscle cells. As to the mechanistic aspects, it is suggested that an increase in extracellular Pi triggers signal transduction via the PiT1 type III sodium/phosphate (Na^+/Pi) cotransporter and ERK1/2 pathway. Unicellular organisms such as bacteria and yeast sense the environmental Pi with a protein complex located in the plasma membrane, which regulates the expression of multiple genes involved in Pi uptake and metabolism to adapt to its availability. In mammals that are multicellular organisms, Pi availability should be sensed both at a cellular level to regulate the function of each cell and as a whole body to maintain the Pi homeostasis of the extracellular fluid. Although the responsiveness to the increased extracellular Pi suggests the existence of Pi-sensing mechanism in mammalian cells as well, it is unknown whether the sensing of Pi availability at a cellular level and that at a whole-body level share the same pathway or not. This chapter will review the findings regarding the regulation of various cellular functions by extracellular Pi, and also discuss the current concept on the mechanism for Pi-sensing.

Phosphorus is critical in various biological processes including membrane integrity, synthesis of deoxyribonucleic acid (DNA) and ribonucleic acid (RNA), energy metabolism and intracellular signaling. In vertebrates, phosphorus is also

essential in skeletal mineralization. In human adults, approximately 85% of the total phosphorus exists in bone as complex with calcium in hydroxyapatite crystals deposited onto the collagen matrix. Fifteen percent of phosphorus is present in soft tissues with only 0.1% in the extracellular fluids [1]. Phosphorus in serum is present mainly as inorganic phosphate (Pi) in the form of free ions HPO_4^{2-} and $H_2PO_4^-$, and the former is dominant in physiological pH. The majority of the intracellular phosphate ion exists as bound form or inorganic phosphate esters, phospholipids, or phosphorylated intermediate molecules involved in various biochemical processes. The concentration of Pi in the extracellular fluid and cytosol is about 10^{-4} and 2×10^{-4} M, respectively. The intracellular concentration of Pi is maintained by membrane transporters, which function dependently on sodium (Na^+) gradient across the plasma membrane [1].

In mammals, Na^+-coupled Pi cotransporters have been classified into three families, based on the amino acid sequence and structural similarity [2]. All cotransporters are multispanning membrane proteins. The type I Na^+/Pi cotransporter belongs to the solute carrier family 17 (SLC17), and is known as NPT1 in humans. In addition to the Pi transport activity, type I cotransporters transport organic anions, and their physiological roles are not fully established. Type II Na^+/Pi cotransporters are assigned to SLC34, and include NPT2a, NPT2b and NPT2c. Npt2a and Npt2c were shown to be predominantly expressed at the brush border membrane of proximal tubular epithelial cells, and responsible for the renal reabsorption of Pi. On the other hand, Npt2b is expressed in various tissues including small intestine, and has been revealed to be responsible for intestinal apical Na^+/Pi cotransport. Type III Na^+/Pi cotransporters are classified as SLC20 family, which includes PiT1 (SLC20A1) and PiT2 (SLC20A2). These proteins are widely expressed, and were originally identified as retroviral receptors Glvr-1 and Ram-1, respectively [2].

In addition to the profound roles of phosphorus in various biological processes, it has been implicated that extracellular Pi itself functions as a signaling molecule that regulates gene expression and modulates cell behavior. This chapter will review the recent findings on the regulation of cellular function by extracellular Pi. In addition, current concept on the sensing mechanism of environmental Pi will be discussed.

Roles of Extracellular Pi in Skeleton

In mammals, renal reabsorption and intestinal absorption of Pi are central to control Pi balance [1]. Prolonged deficiency of Pi due to the abnormal absorption or reabsorption results in the poorly mineralized bone characteristic of rick-

Razzaque MS (ed): Phosphate and Vitamin D in Chronic Kidney Disease.
Contrib Nephrol. Basel, Karger, 2013, vol 180, pp 14–24 (DOI: 10.1159/000346776)

ets or osteomalacia, indicating the critical role of phosphorus in skeletal mineralization. Recently, it has been revealed that extracellular Pi regulates the various cellular functions in skeleton other than mineralization.

Alkaline phosphatase is the enzyme that hydrolyses pyrophosphates and the protein-bound form of phosphate to produce Pi and increase its concentration in the extracellular microenvironment. During the early phase of osteoblast differentiation, the expression of the gene for alkaline phosphatase gradually increases. Using a murine osteoblastic cell line MC3T3-E1 cells, Beck et al. [3] found that a decrease in extracellular Pi production due to the inhibition of alkaline phosphatase activity caused a decreased expression of osteopontin, which is involved in the regulation of mineralization. Then, they further demonstrated that the increased Pi levels in the culture medium strongly induced the expression of osteopontin, and firstly indicated that extracellular Pi itself functions as a specific signal that regulates the gene expression in osteoblastic cells [4]. The authors also performed a combined proteome and microarray investigation in MC3T3-E1 cells to identify the molecules comprehensively whose expression levels were altered in response to treatment with the higher concentration of extracellular Pi [5]. Among the molecules whose amount was increased in response to Pi, some were found to be involved in the regulation of cell cycle, proliferation and DNA synthesis [5]. Thus, the extracellular Pi in microenvironment seems to regulate both proliferation and differentiation of osteoblasts.

Extracellular Pi plays a role in regulating chondrogenesis as well. Chondrogenesis is a multistep process involving the mesenchymal condensation of undifferentiated cells, the proliferation of chondrocytes, and differentiation into hypertrophic chondrocytes, followed by mineralization. As chondrocytes mature, the concentration of Pi increases in the extracellular milieu. The progressive accumulation of Pi ion starts from the proliferative zone and peaks in the hypertrophic zone [6].

Terminally differentiated chondrocytes in growth plate undergo mineralization associated with apoptosis. Several studies have indicated that high level of Pi in the microenvironment of mature chondrocytes induces apoptosis [7–9]. Sabbagh et al. [7] demonstrated that the decreased level of extracellular Pi impaired the apoptosis of hypertrophic chondrocytes and lead to rickets in the hypophosphatemic *Hyp* mouse, a murine model for human X-linked hypophosphatemia. Their data implicate that extracellular Pi plays a critical role for the regulated apoptosis of hypertrophic chondrocytes via the activation of the caspase-9-mediated mitochondrial pathway. Mansfield et al. [8] linked the apoptosis of mature chondrocytes directly to the elevation in environmental Pi concentration and the concomitant rise in intracellular Pi levels, and showed that the effect of Pi on chondrocyte apoptosis was calcium dependent. More recently, Sugita et al. [9] reported that Pi-regulated apoptosis of hypertrophic

Razzaque MS (ed): Phosphate and Vitamin D in Chronic Kidney Disease.
Contrib Nephrol. Basel, Karger, 2013, vol 180, pp 14–24 (DOI: 10.1159/000346776)